Lithos 326–327 (2019) 313–326

Contents lists available at ScienceDirect

Lithos

journal homepage: www.elsevier.com/locate/lithos

Garnet Lu—Hf geochronology and P-T path of the Gridino-type eclogite in the Belomorian Province, Russia

Huanglu Yu [a], Lifei Zhang [a,*], Pierre Lanari [b], Daniela Rubatto [b], Xiaoli Li [a]

[a] MOE Key Laboratory of Orogenic Belt and Crustal Evolution, School of Earth and Space Sciences, Peking University, Beijing 100871, China
[b] Institute of Geological Sciences, University of Bern, Bern 3012, Switzerland

ARTICLE INFO

Article history:
Received 6 September 2018
Accepted 22 December 2018
Available online 28 December 2018

Keywords:
Lu—Hf Geochronology
Gridino-type eclogite
Phase equilibria modeling
P-T path
Paleoproterozoic

ABSTRACT

Eclogites are commonly seen as markers of subduction and thus their presence in Proterozoic and Archean orogenic provinces is crucial information for determining the initiation of modern plate tectonic. The Belomorian province hosts some of the oldest known eclogite-facies rocks. Here we present new garnet Lu—Hf geochronology that constrains the prograde stage of Gridino-type eclogite to ca. 1.96–1.92 Ga. Inherited magmatic zircon cores have $^{176}Hf/^{177}Hf$ ratios that indicate isotopic disequilibrium between the inherited zircon cores and the metamorphic mineral assemblages, while the metamorphic rims have variable $^{176}Hf/^{177}Hf$ ratios that reflect Paleoproterozoic eclogite-facies metamorphism. Iterative thermodynamic models, involving the optimization of pressure (P), temperature (T) and reactive bulk composition (X) was used to reconstruct the P-T conditions recorded by garnet, and define the prograde trajectory. Zr-in-rutile thermometry, combined with equilibrium phase diagrams, constrains the peak P-T conditions at 725–750 °C and above 18 kbar, corresponding to an average apparent thermal gradient of below 41 °C/kbar. The P-T conditions of the high-pressure granulite facies overprint are 680–730 °C at 9–10 kbar. Thus, the metamorphic evolution of Gridino-type eclogite followed a clockwise P-T path with a cooling decompression stage, recording the assembly of the Columbia supercontinent during the Paleoproterozoic.

1. Introduction

Eclogite facies rocks are characteristic products of high-pressure metamorphism in subduction zones (Brown, 2006; Carswell, 1990), and as such are regarded as important indicators of modern plate tectonics (e.g. Brown, 2006, 2008, 2014; Condie and Kröner, 2008; Miyashiro, 1961), although a lower crustal delamination origin has also been proposed for some eclogites that decipher early-Earth tectonics (Johnson et al., 2014; Stern, 2008). Paleoproterozoic high-pressure rocks are globally widespread, including the Trans-Hudson eclogite (Weller and St-Onge, 2017), the Snowbird eclogite (Baldwin et al., 2007), the Slave eclogite (Smart et al., 2014, 2016), the Usagaran and Ubendian eclogite (Boniface et al., 2012; Collins et al., 2004), the Eburnian-Transamazonian eclogite (Loose and Schenk, 2018),the Trans-North China eclogite (Xu et al., 2017) and the Belomorian eclogite (Imayama et al., 2017; Li et al., 2017a; Liu et al., 2017; Yu et al., 2017). These occurrences suggest that plate tectonic processes comparable to modern ones have operated at least since the Paleoproterozoic. Reconstructing the detailed P-T-t evolution of these high-pressure rocks directs implications for early plate tectonics.

Linking the timing of metamorphic events to specific thermal histories is fundamental to reconstruct the geodynamic evolution of orogenies (e.g. Engi et al., 2017). Garnet is common in high-pressure rocks and particularly important, because it can be dated by Lu—Hf geochronology (Cheng et al., 2008; Duchêne et al., 1997; Lapen et al., 2003; Scherer et al., 2000) and its major element composition can constrain quantitative P-T paths (Hernández-Uribe et al., 2018; Lanari et al., 2017). The relatively high closure temperature for the Lu—Hf system (Dodson, 1973; Philippot et al., 2001; Scherer et al., 2000; Smit et al., 2013) makes this dating method particularly suitable for middle- to high-grade rocks. Additionally, Lu—Hf garnet geochronology is insensitive to light rare earth element (LREE)-rich inclusions in garnet, such as epidote, which are critical contaminants for Sm—Nd geochronology (Anczkiewicz and Thirlwall, 2003; Scherer et al., 2000). Lu—Hf garnet technique can be used to constrain the prograde and middle-high temperature history of orogens (e.g. Cheng et al., 2008; Kylander-Clark et al., 2007; Lagos et al., 2007; Lapen et al., 2003; Scherer et al., 2000). Furthermore, garnet porphyroblasts with compositional zoning can be used to reconstruct part of the P-T history (e.g. Cheng et al., 2015; Gaidies et al., 2008; Spear and Selverstone, 1983). Based on garnet compositions obtained from quantitative compositional maps, garnet growth can be modeled through distinct P-T stages involving garnet fractionation and/or resorption (Lanari et al., 2017).

* Corresponding author.
E-mail address: lfzhang@pku.edu.cn (L. Zhang).

https://doi.org/10.1016/j.lithos.2018.12.032
0024-4937/© 2018 Published by Elsevier B.V.

Although an Archean age (2.87–2.72 Ga) has been ascribed to the Belomorian eclogite (Dokukina et al., 2014; Li et al., 2015; Mints et al., 2010, Mints et al., 2014), eclogite facies metamorphism in the Belomorian eclogites, both the Gridino- and Salma-type eclogites, has been dated to be ca. 1.90 Ga using zircon U—Pb geochronology (Imayama et al., 2017; Li et al., 2017a; Liu et al., 2017; Yu et al., 2017) and ca. 1.89–1.94 Ga by garnet Lu—Hf geochronology (Berezin et al., 2012; Herwartz et al., 2012). This contribution focuses on the Gridino-type eclogite in the Belomorian province. We report garnet Lu—Hf geochronology for four eclogites, and zircon Hf isotopes of two samples. These data allow us to constrain the timing of the peak metamorphism in the Belomorian Province. Based on the detailed petrography study of sample Gd 10, we model garnet growth and obtain the prograde trend using $G_{RT}M_{OD}$ (Lanari et al., 2017). We constrain the peak P-T conditions and the retrograde P-T stage combining phase equilibria modeling and Zr-in-rutile thermometer or Hbl-Pl thermometer, thus adding more precise constraints to the evolution of Gridino-type eclogite than the previous work (e.g. Li et al., 2015; Perchuk and Morgunova, 2014; Yu et al., 2017).

2. Geological background

The Belomorian province is a NW-trending metamorphic belt over 500 km long and 50–60 km wide in the southwestern foreland of the Paleoproterozoic Lapland-Kola collisional orogen (Fig. 1a, b). The major lithological components of the Belomorian Province are the 2.9–2.7 Ga tonalite–trondhjemite–granodiorite (TTG) gneisses that were metamorphosed in the Paleoproterozoic (Hölttäs et al., 2008), the 2.95 Ga paragneisses (Hölttäs et al., 2008; Slabunov et al., 2006), 3.1–2.7 Ga greenstones and the Paleoproterozoic Gridino- and Salma- type eclogites which occur as lenticular bodies within the TTG gneisses (Hölttäs et al., 2008; Slabunov et al., 2006). Gridino-type eclogites were originally gabbroic dikes intruding TTG gneisses, which underwent coeval eclogite facies metamorphism (Yu et al., 2017), while the Salma-type eclogites are the product of high-pressure metamorphism of oceanic lithosphere (Imayama et al., 2017; Mints et al., 2014). The Belomorian Province was intruded by several magmatic suites ranging in age from Neoarchean to Paleoproterozoic at 2.72–2.70 Ga, 2.5–2.4 Ga, and 2.1–1.9 Ga (Dokukina et al., 2014; Mints et al.,

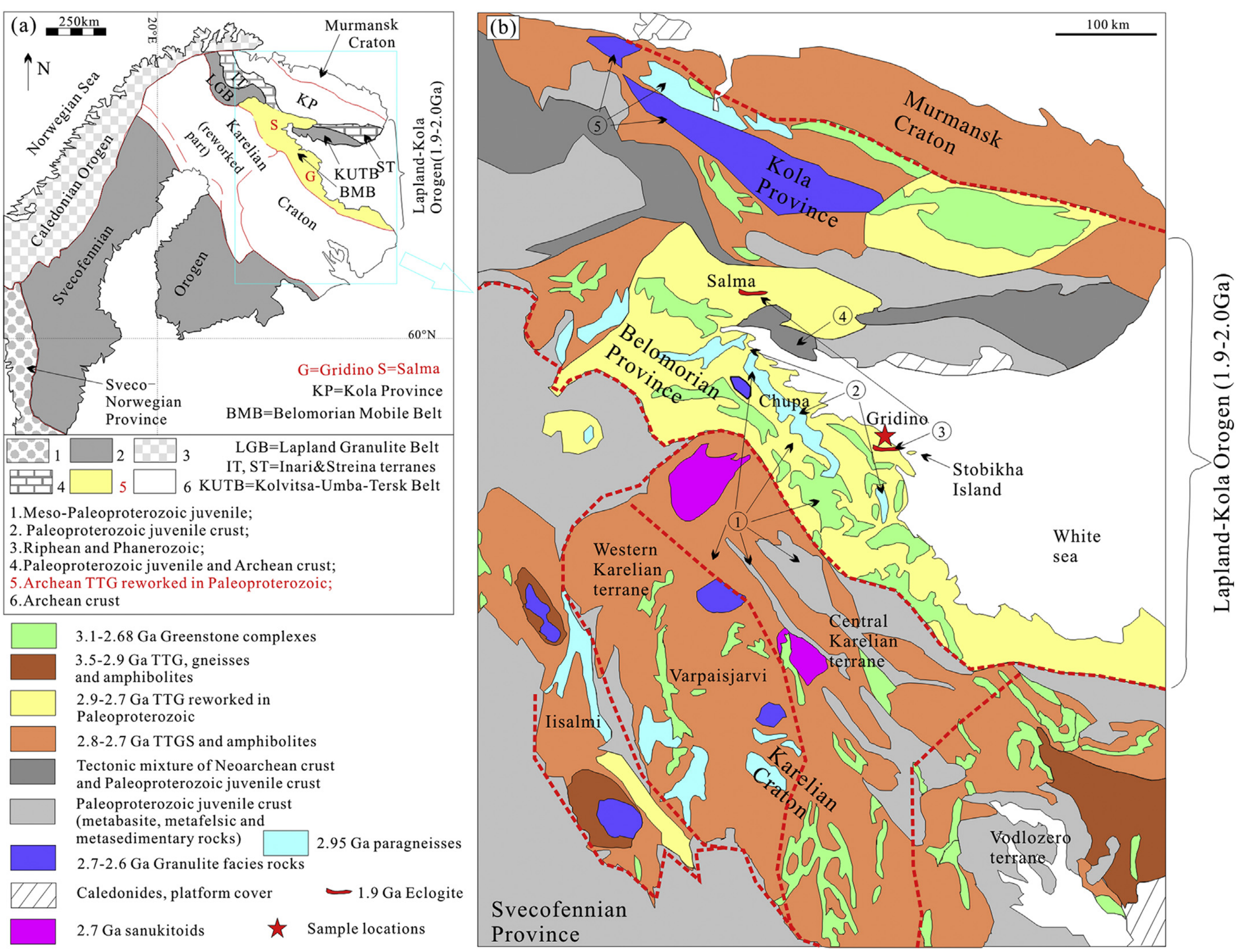

Fig. 1. (a) Simplified geological maps of the Fennoscandian shield. Modified after Daly et al. (2006) and Mudruk et al. (2013); (b) Detailed geological map of the Paleoproterozoic Lapland-Kola orogen. Modified after Yu et al., 2017. Circled numbers summarize previous geochronological results: ① Titanite and rutile U—Pb ages of 1.9–1.8 Ga in metabasic, metafelsic, and metasedimentary rocks, as well as TTG and greenstones (Bibikova et al., 2001; Nesterova et al., 2011);② Paragneisses with an depositional age of ca. 2.95 Ga (Balagansky, 2002) and metamorphosed at 1.9–1.8 Ga (Ruchyev, 2000);③ Eclogites with a protolith age of >2.7 Ga and metamorphosed at 1.9 Ga (Skublov et al., 2011a, 2011b); Eclogites with a Grt Lu—Hf age of 1.9 Ga (Herwartz et al., 2012); titanite age of 1.88–1.86 Ga for amphibolite facies metamorphism (Skublov et al., 2014; Yu et al., under review); ④ Tectonic assemblage of 2.8 Ga gneiss, 2.32 Ga schist and 1.90 Ga granodiorites (Korikovsky et al., 2014);⑤ Archean terranes reworked during the Paleoproterozoic Lapland-Kola collisional orogeny (Hölttäs et al., 2008; Slabunov et al., 2006).

2014; Skublov et al., 2011a, 2011b; Stepanova et al., 2014). The collision of Paleoproterozoic juvenile crust in the orogenic core with the surrounding Belomorian and Kola Provinces led to the formation of the Lapland-Kola collisional orogeny at 1.93–1.91 Ga (Daly et al., 2006). The final product is a mixed basement that records a polyphase deformation history.

A tectonic mélange zone extends from NW to SE along the White Sea coast, and is exposed near the Gridino village and adjacent islands (Fig. 1b). Regional geological mapping and field observations suggest that the mélange zone consists of a mixture of TTG gneisses, paragneisses, diverse metabasic rock boudins and numerous metamorphosed dykes that range from undeformed to strongly deformed ones (Mints et al., 2014; Slabunov et al., 2006; Yu et al., 2017). The undeformed dykes retain intrusive contact with the TTG gneisses, while the intensely deformed dykes consist of lenses or boudins ranging from tens of centimeters to several meters across that are concordant with the foliation of the host gneiss (Mints et al., 2014; Slabunov et al., 2006; Yu et al., 2017). These metamorphosed dykes are mainly from gabbro and norite protoliths and metamorphosed under eclogite-facies conditions (Dokukina et al., 2014; Mints et al., 2014).

Despite early claims of Archean metamorphism, recent studies have established that the Belomorian eclogites are Paleoproterozoic (Imayama et al., 2017; Li et al., 2017a, 2017b; Liu et al., 2017; Yu et al., 2017). The Gridino-type eclogite have been dated using zircon U—Pb geochronology (Skublov et al., 2011a; Yu et al., 2017). Zircon rims yield U—Pb ages of ca. 1.90 Ga, interpreted to reflect eclogite facies metamorphism, while zircon cores have Neoarchean U—Pb ages of ca. 2.70 Ga, ascribed to the formation of the magmatic protolith (Skublov et al., 2011a; Yu et al., 2017). The garnet Lu—Hf isochron ages of the corresponding eclogites from the same area are ca. 1.89 Ga and 1.94 Ga (Herwartz et al., 2012), which are consistent with the ages obtained from the zircon rims. The ages of adjacent Salma-type eclogite have also been constrained to be ca. 1.90 Ga with multiple geochronometers, such as zircon U—Pb geochronology, garnet Lu—Hf and Sm—Nd geochronology (Herwartz et al., 2012; Imayama et al., 2017; Liu et al., 2017; Skublov et al., 2011b).

3. Petrography and mineral chemistry

Electron probe micro-analyses (EPMA) were performed using a JEOL JXA-8200 at the Institute of Geological Sciences of the University of Bern and a JEOL JXA-8100 at the Peking University. The EPMA session includes two parts, X-ray compositional maps and the measurement of point analyses. Analytical conditions for X-ray maps were 15 KeV accelerating voltage, 100 nA specimen current and 200 ms dwell times. Nine elements (Si, Ti, Al, Fe, Mn, Mg, Na, Ca and K) were measured at the specific wavelength in two passes. Intensity maps were standardized using spot analyses as internal standard. X-ray maps were calibrated to oxide mass concentrations using XM$_{AP}$T$_{OOLS}$ 2.2.1 (Lanari et al., 2014). Analytical conditions for point analyses were 15 KeV accelerating voltage, 20 nA specimen current and 40 s dwell times. The detailed analytical procedures are described in Lanari et al. (2013, 2017) and Li et al. (2017c).

Four eclogite samples have been collected, two samples from eclogite boudins on Stolbikha Island (Gd 07 and Gd 10), one sample from an undeformed metamorphosed dyke near Gridino village (Gd 32) and one sample from an eclogite boudin on Vycokiy Island (Gd 19). Three of them (Gd 07, Gd 10 and Gd 32) have been presented in Yu et al. (2017), including the petrography and zircon U—Pb geochronology. This paper focuses on two samples in petrography, Gd 10 and Gd 19. The coordinates, main mineral assemblages and prior metamorphic zircon ages of these samples are listed in Table 1. In an attempt to better constrain the metamorphic evolution of the Gridino-type eclogite, we also provide quantitative compositional maps for sample Gd 10. Mineral abbreviations follow Whitney and Evans (2010).

3.1. Sample Gd 10

This sample shows a porphyroblastic texture. The mineral assemblages are garnet (40 vol%), omphacite (40 vol%), hornblende (10 vol%), diopside+plagioclase forming symplectite around omphacite (5 vol%) and rutile (5 vol%). The phase map and compositional maps of two representative areas are shown in Fig. 2a, b. Garnet is euhedral-subhedral and 0.5–1.0 mm in diameter. They have homogeneous compositions in cores ($Alm_{40–46}$ $Prp_{21–25}$ $Grs_{27–32}$ Sps_1; Fig. 3, Table 2), whereas thin rims contain higher pyrope ($Prp_{23–26}$) and lower grossular ($Grs_{23–27}$) contents (Fig. 3, Table 2). Inclusions of diopside, plagioclase, hornblende and quartz are observed in garnet cores. Two types of clinopyroxene were identified in this sample. The cores of coarse-grained clinopyroxene have high jadeite content (J_O 30–32, (Na)M2 in Clinopyroxene) (Fig. 4), which is omphacite. While the rims of coarse-grained clinopyroxene and the fine-grained clinopyroxene in the symplectite are diopside (J_O 9) (Fig. 4, Table 2). Plagioclase in symplectite are slightly zoned from core (An_{26}) to rim (An_{24}) (Table 2). Two types of hornblende were also identified. One type is systematically enclosed in the garnet grains (compositions are given in Yu et al., 2017). The other type occurs in the symplectitic domains and exhibits higher Fe and lower Ti contents (Table 2). Rutiles are included in omphacite, metamorphic zircon rim (Yu et al., 2017) or paragenetic with omphacite.

3.2. Sample Gd 19

The sample displays a porphyroblastic texture and mainly comprises of garnet (60 vol%), omphacite (30 vol%) and kyanite (10 vol%), with little diopside+plagioclase symplectite (Fig. 5). Garnet porphyroblasts are euhedral-subhedral and 1.5–2.0 mm in diameter. The core of these garnet crystals is rich in fine-grained quartz inclusions, while mantle and rim are inclusion poor. Most garnet grains show weak compositional zoning (Fig. 6, profile A to B, labelled in Fig. 5a; Table 3). The core is slightly more Grs rich ($Alm_{39–41}Prp_{36–38}Grs_{20–22}Sps_1$) whereas towards the mantle, pyrope content increases, while grossular content decreases slightly ($Alm_{39–42}Prp_{39–41}Grs_{19–20}Sps_1$). At the rim, pyrope and grossular contents decrease, almandine content increases ($Alm_{40–42}Prp_{38–39}Grs_{19–20}Sps_1$). Omphacite is euhedral to subhedral with small grain size (0.1–0.2 mm). The J_O value of the omphacite is 21–23. (Table 3). Kyanite grains are subhedral, 0.5 mm in diameter and occur as aggregates.

4. Lu—Hf geochronology

Determination of Lu and Hf isotope ratios were carried out in static mode on Faraday cups using a Thermo Fisher Scientific Neptune MC-ICP-MS at the Institute of Geology and Geophysics (IGG), Chinese Academy of Sciences (CAS), Beijing. Garnet, omphacite and kyanite were

Table 1
Coordinates, main mineral assemblages and prior zircon ages of investigated samples.

Sample names	Coordinates	Main mineral assemblages	Metamorphic zircon ages
Gd07	N 65°52′41.43″/E 34°50′54.25″	Grt + Omp + Ky + Hbl + (Di + Pl) sympletite+Rt	1904.2 ± 4.1 Ma (Yu et al., 2017)
Gd10	N 65°52′43.62″/E 34°50′58.53″	Grt + Omp + Ky + Hbl + (Di + Pl) sympletite+Rt	1898.6 ± 5.3 Ma (Yu et al., 2017)
Gd32	N 65°55′20.34″/E 34°41′58.29″	Grt + Omp + Hbl + Rt	1970 ± 42 Ma (Yu et al., 2017)
Gd19	N 65°56′37.32″/E 34°41′35.39″	Grt + Omp + Ky + (Di + Pl) sympletite+Rt	Not reported

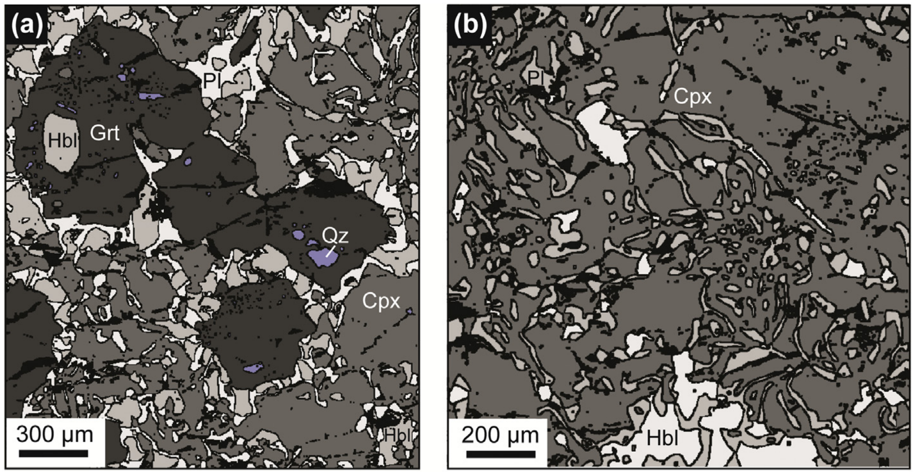

Fig. 2. Mineral distribution in the mapped area obtained using the multi-channel classification method in XMapTools (Lanari et al., 2014). The different color represent different mineral phases; black pixels are holes or mixed pixels filtered using the BRC correction of XMapTools (Lanari et al., 2018).

handpicked under a binocular microscope individually, excluding grains with visible inclusions. Approximately 0.15 g of whole rock, 0.20 g of garnet, 0.20 g of omphacite (used in sample Gd07, Gd10 and Gd 32) or 0.20 g of kyanite (used in sample Gd19) were digested for each geochronological point. Sample dissolution, chemical separations, and isotopic analysis protocols follows Yang et al. (2010). Hf isotope analyses

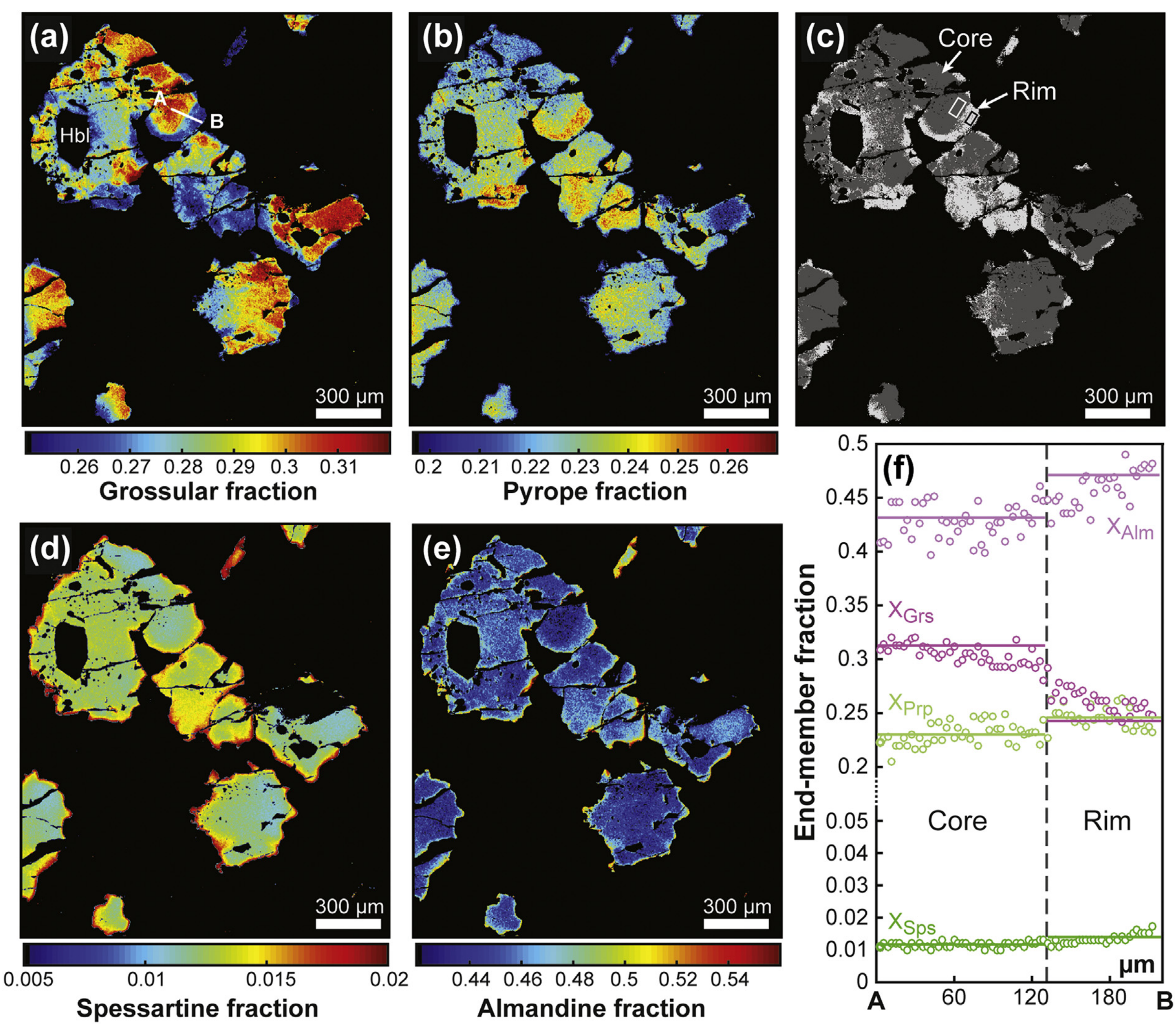

Fig. 3. Garnet compositional maps in sample Gd 10. Data obtained using XMapTools: maps of end-member proportions (a) grossular; (b) pyrope; (d) spessartine; (e) almandine. (c) Maps of the compositional groups. (f) Compositional zoning profile of garnet (between A and B, the profile position is reported in (a)).

Table 2
Representative electron microprobe analyses of minerals in sample Gd10.

core-rim												
Mineral	Grt(core)	Grt(rim)	Grt(rim)		Di	Di		Pl(core)	Pl(rim)	Pl(rim)	Hbl	Hbl
SiO2(wt%)	38.38	38.6	38.81		51.78	51.84		61.42	62.52	61.19	44.35	44.35
TiO2	bdl	bdl	0.03		0.04	0.30		bdl	bdl	bdl	0.56	0.76
Al2O3	21.38	21.31	21.39		3.83	4.02		23.73	23.22	23.13	12.46	12.43
Cr2O3	0.15	bdl	0.11		0.09	0.27		0.04	0.03	bdl	0.13	0.16
FeO	22.26	23.48	23.07		7.39	7.28		0.17	0.13	0.16	12.12	12.85
MnO	0.46	0.60	0.49		0.14	0.08		0.03	bdl	bdl	0.13	0.06
MgO	6.80	7.37	7.20		12.71	12.63		bdl	0.02	bdl	13.20	12.69
CaO	9.54	8.16	9.01		21.78	22.46		5.25	4.92	4.92	10.90	11.05
Na2O	0.01	bdl	0.01		1.30	1.31		8.30	8.73	8.52	2.52	2.39
K2O	bdl	bdl	bdl		bdl	bdl		0.07	0.13	0.15	0.33	0.35
NiO	0.09	0.08	0.00		bdl	bdl		bdl	bdl	bdl	bdl	0.05
Total	99.07	99.60	100.12		99.06	100.19		99.03	99.71	98.09	96.70	97.13
Si (apfu)	2.98	2.98	2.98		1.93	1.91		2.75	2.78	2.76	6.49	6.49
Ti	0.00	0.00	0.00		0.00	0.01		0.00	0.00	0.00	0.06	0.08
Al	1.96	1.94	1.94		0.17	0.18		1.25	1.22	1.23	2.15	2.15
Cr	0.01	0.00	0.01		0.00	0.01		0.00	0.00	0.00	0.02	0.02
Fe3	0.08	0.10	0.10		0.07	0.08		0.01	0.01	0.01	0.34	0.30
Fe2	1.37	1.42	1.38		0.16	0.15		0.00	0.00	0.00	1.15	1.27
Mn	0.03	0.04	0.03		0.00	0.00		0.00	0.00	0.00	0.02	0.01
Mg	0.79	0.85	0.82		0.71	0.69		0.00	0.00	0.00	2.88	2.77
Ca	0.79	0.68	0.74		0.87	0.89		0.25	0.23	0.24	1.71	1.73
Na	0.00	0.00	0.00		0.09	0.09		0.72	0.75	0.75	0.72	0.68
K	0.00	0.00	0.00		0.00	0.00		0.00	0.01	0.01	0.06	0.07
(mole fraction)												
Alm	0.46	0.48	0.46	J_O	9	9	An	0.26	0.24	0.24		
Sps	0.01	0.01	0.01									
Prp	0.26	0.28	0.28									
Grs	0.27	0.23	0.25									

bdl = below detection limit; $^*J_O$ = (Na)M2 in Clinopyroxene; An = Ca/(Ca + Na) in Plagioclase.

consist of 9 blocks of 10 cycles per block with an intergration time of 4 s per cycle. Analyses of JMC 475 yielded the $^{176}Hf/^{177}Hf$ values within uncertainties recommended by Blichert-Toft et al. (1997). Hafnium isotopic composition were corrected for mass fractionation with an exponential law using $^{179}Hf/^{177}Hf = 0.7325$. Hf concentrations were calculated from the corrected $^{180}Hf/^{177}Hf$ mixture ratio, using the isotope dilution equation. External uncertainties applied to measured data are 1% for $^{176}Lu/^{177}Hf$ and a blanket 0.005% uncertainty added in quadrature for $^{176}Hf/^{177}Hf$. Lu—Hf ages were calculated using the ^{176}Lu decay constant of 1.867^*10^{-11} (Scherer et al., 2001) and isochrons were produced using the program Isoplot 4.11 (Ludwig, 2012). Errors are reported at 95% confidence level.

Isochrons were constrained by whole-rock, garnet, omphacite or kyanite aliquots (Table 4). Garnet separates show Lu—Hf ratios of 1.96–5.18, $^{176}Lu/^{177}Hf$ ratios of 0.2785–0.7401 and $^{176}Hf/^{177}Hf$ ratios of 0.291654–0.306630. Omphacite separates have Lu—Hf ratios of 0.03–0.05, $^{176}Lu/^{177}Hf$ ratios of 0.0037–0.0059 and $^{176}Hf/^{177}Hf$ ratios of 0.281834–0.281890. Whole-rock separates show Lu—Hf ratios of 0.33–0.55, $^{176}Lu/^{177}Hf$ ratios of 0.0464–0.0779 and $^{176}Hf/^{177}Hf$ ratios of 0.283095–0.284778. Kyanite separates show Lu—Hf ratios of 0.01, $^{176}Lu/^{177}Hf$ ratios of 0.0018 and $^{176}Hf/^{177}Hf$ ratios of 0.281195.

The whole-rock aliquot, garnet and omphacite fractions from eclogite boudin Gd 07 define a regression that yields a Lu—Hf isochron age of 2076 ± 39 Ma, with a MSWD of 0.15 (Fig. 7a). The whole-rock,

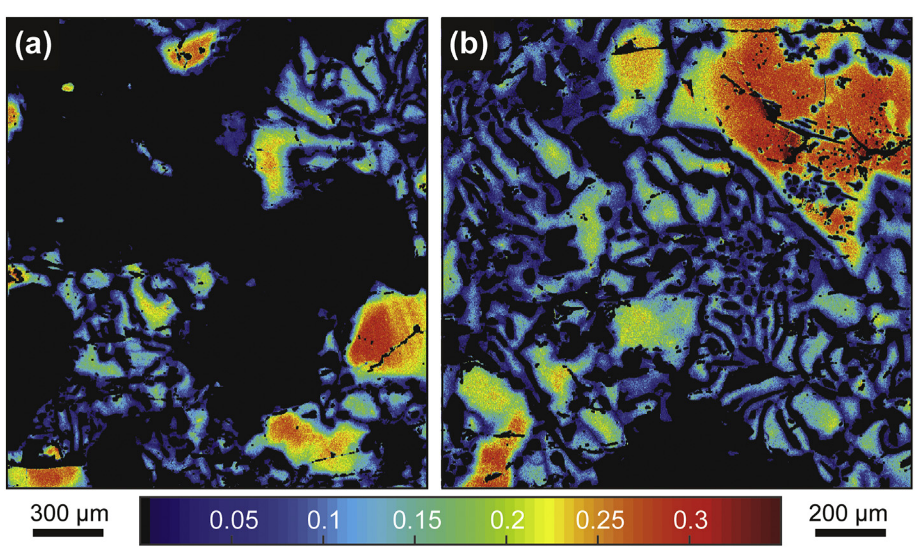

Fig. 4. Maps of J_O in clinopyroxene for sample Gd10, J_O = (Na)M2 in Clinopyroxene.

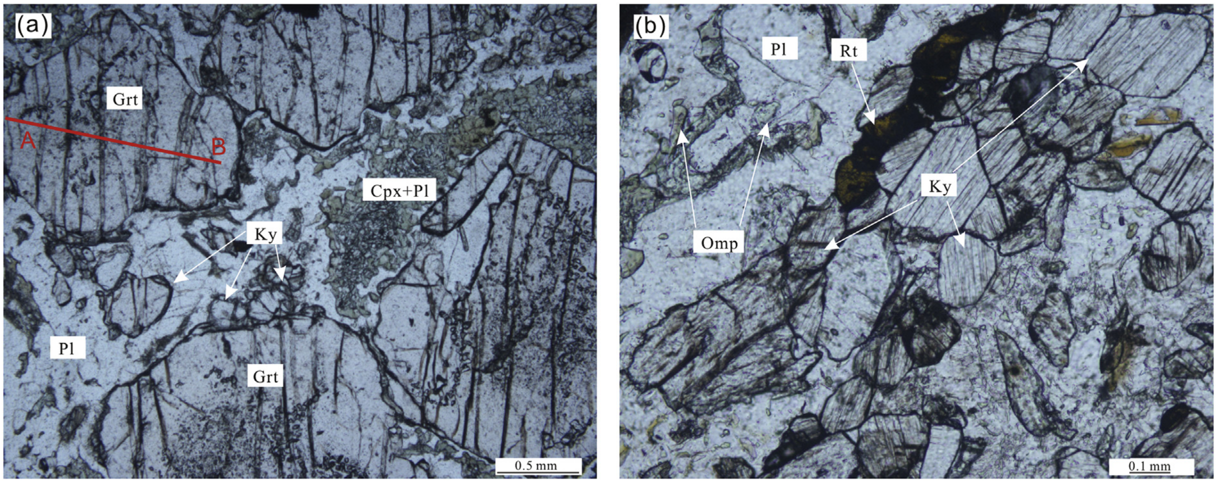

Fig. 5. Photomicrographs of sample Gd 19 showing porphyroblastic texture (a), and kyanite aggregates (b).

garnet and omphacite fractions from eclogite boudin Gd 10 yield a younger Lu—Hf isochron age of 1961 ± 31 Ma, with a MSWD of 0.025 (Fig. 7b). Whole-rock, garnet and kyanite aliquots from eclogite boudin Gd 19 yield a Lu—Hf isochron age of 1917 ± 34 Ma, with a MSWD of 1.3 (Fig. 7c). Eclogite dyke Gd 32 returns a Lu—Hf isochron age of 1871 ± 83 Ma, which is defined by the whole-rock, garnet and omphacite fractions with a MSWD of 0.12 (Fig. 7d).

5. Zircon Hf isotopes

Zircon separation was performed using conventional heavy liquid and magnetic techniques, then individual grains were handpicked under a binocular microscope. Cathodoluminescence (CL) images, geochronology and geochemistry characteristics of zircons in sample Gd 07, Gd 10 and Gd 32 have been presented in Yu et al. (2017). Zircon in-situ Lu—Hf analyses of samples Gd07 and Gd10 were carried out using a NU plasma 2 MC-ICPMS at the School of Earth and Space Sciences, Peking University. An ArF excimer laser ablation system of Geolas HD (193 nm) was used for laser ablation analysis. Zircon 91,500 was used as an internal standard with a reference value of $^{176}Hf/^{177}Hf$ = 0.282307 ± 31 (2SD) (Wiedenbeck et al., 2010; Wu et al., 2006). Plešovice zircon was used as a secondary standard (Sláma et al., 2008) and the value of $^{176}Hf/^{177}Hf$ = 0.282482 ± 13 (2SD) was obtained. The Lu—Hf isotopes and calculated relevant parameters are listed in Table 5 (zircon ages from Yu et al., 2017).

For sample Gd 07, metamorphic zircon rims and inherited magmatic zircon cores have different Lu—Hf isotope compositions (Table 5). Zircon cores have high $^{176}Lu/^{177}Hf$ ratios of 0.000017–0.000457 and $^{176}Hf/^{177}Hf$ ratios of 0.281071–0.281169,εHf(t) values of −1.3 to 3.3 with T_{DM} values of 2855–2972 Ma. Zircon rims have lower $^{176}Lu/^{177}Hf$ ratios of 0.000002–0.000019 and variable $^{176}Hf/^{177}Hf$ ratios of 0.281290–0.281641, with εHf(t) values of −9.6 to 2.4. Zircon cores and rims plot in distinct groups in the $^{176}Hf/^{177}Hf$- age diagram (Fig. 8).

For sample Gd 10, zircon cores are small and fractured, and no meaningful age data were obtained due to loss of Pb (Yu et al., 2017). Only metamorphic zircon rims were analysed and, similarly to sample Gd 07, they have low $^{176}Lu/^{177}Hf$ ratios of 0.000002–0.000023 and variable $^{176}Hf/^{177}Hf$ ratios of 0.281140–0.281572, with εHf(t) values of −15.3 to −0.2 (Table 5). The two samples overlap in the $^{176}Hf/^{177}Hf$-age diagram (Fig. 8).

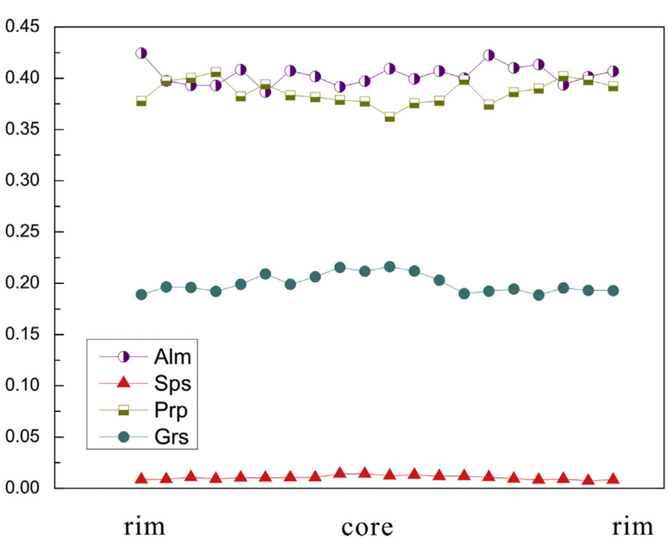

Fig. 6. Representative compositional zoning profile of garnet in sample Gd 19.

6. P-T conditions

Eclogite boudins and metamorphosed dykes in Gridino area are interpreted to experience coeval eclogite facies metamorphism in the Paleoproterozoic. The P-T conditions deciphered in sample Gd 10 are therefore assumed to be representative of the metamorphic evolution of the whole Gridino area.

In attempt to better constrain the P-T evolution of Gridino-type eclogite and the growth conditions of the dated garnet, we provide here new thermodynamics modeling based on quantitative compositional mapping results for sample Gd 10. The P-T conditions recorded by garnet of sample Gd 10 were obtained using an iterative thermodynamic model and the program GrtMod (Lanari et al., 2017). The internally consistent database of tc55 from Powell et al. (1998; updated October 2009) was used along with the following activity-composition relations: garnet (Holland and Powell, 1998), clinopyroxene (Green et al., 2007), epidote (Holland and Powell, 1998), plagioclase (Holland and Powell, 2003), amphibole (Diener et al., 2007), ilmenite (White et al., 2001), and orthopyroxene (White and Powell, 2002). Kyanite, lawsonite, rutile, coesite and quartz are pure end-member phases. P_2O_5 was neglected because it is only bounded in the accessory mineral apatite, and the corresponding CaO was excluded from the bulk rock composition. MnO was also ignored for its low abundance and the small effect of Mn on phase equilibria at these conditions. H_2O is considered to be in excess. The bulk compositions used in the calculation is SiO_2 = 50.99, Al_2O_3 = 8.01, CaO = 14.40, MgO = 14.03, FeO = 9.07,

Table 3
Representative electron microprobe analyses of garnet and omphacite in sample Gd 19.

	rim-core-rim																						
Mineral	Grt (rim)	Grt	Grt	Grt	Grt	Grt	Grt	Grt	Grt	Grt (core)	Grt	Grt	Grt	Grt	Grt	Grt	Grt	Grt	Grt	Grt (rim)		Omp	Omp
SiO2(wt%)	39.84	39.77	39.89	39.82	40.13	39.83	40.08	39.99	39.68	40.00	40.01	39.90	39.81	39.95	39.70	40.11	40.15	40.04	40.31	40.01		52.61	52.03
TiO2	0.03	0.02	bdl	0.01	0.07	0.08	0.04	0.03	bdl	0.11	0.08	0.03	0.07	0.01	bdl	0.08	0.07	bdl	bdl	0.03		0.14	0.15
Al2O3	22.06	22.18	21.99	21.68	22.00	21.95	21.97	22.04	22.00	22.02	21.94	21.75	21.62	21.94	21.86	21.72	21.86	21.88	21.89	21.71		7.07	7.50
Cr2O3	0.02	0.05	0.11	0.05	0.01	bdl	0.07	0.03	0.04	0.01	bdl	bdl	0.01	0.02	0.07	0.03	0.03	0.04	0.06	0.03		0.08	0.09
FeO	20.61	20.07	20.11	20.12	20.19	20.03	19.97	19.77	20.15	20.12	19.99	20.49	20.25	20.71	20.46	20.71	20.56	20.46	20.09	20.45		6.87	6.78
MnO	0.41	0.41	0.50	0.43	0.49	0.49	0.51	0.51	0.66	0.67	0.58	0.61	0.57	0.56	0.51	0.44	0.40	0.43	0.34	0.40		0.12	0.04
MgO	10.03	10.60	10.68	10.77	10.27	10.53	10.31	10.24	10.05	10.12	9.71	10.07	10.11	10.64	9.95	10.41	10.46	10.79	10.74	10.52		11.08	10.93
CaO	6.99	7.29	7.27	7.09	7.43	7.77	7.45	7.70	7.95	7.89	8.06	7.89	7.55	7.05	7.12	7.29	7.04	7.29	7.25	7.21		18.76	18.34
Na2O	0.05	0.01	0.02	0.06	0.04	bdl	bdl	bdl	0.03	0.03	0.03	bdl	bdl	0.04	0.01	bdl	0.03	0.01	0.02	bdl		3.00	3.15
K2O	0.03	bdl	0.02	0.02	bdl	0.02	bdl	bdl	0.01	bdl	bdl	bdl	bdl	bdl	0.01	bdl	0.03	bdl	0.01	0.01		bdl	0.01
NiO	0.02	bdl	bdl	bdl	bdl	bdl	bdl	bdl	bdl	0.02	bdl	bdl	0.05	bdl	0.01	0.01	0.05	bdl	0.01	bdl		0.03	bdl
Total	100.009	100.40	100.58	100.05	100.64	100.70	100.40	100.30	100.57	101.0	100.40	100.74	100.04	100.91	99.69	100.80	100.68	100.94	100.71	100.37		99.75	99.01
Si (apfu)	3.01	2.98	2.99	2.99	3.01	2.98	3.01	3.00	2.98	2.99	3.01	2.99	3.01	2.98	3.01	3.00	3.01	2.99	3.01	3.01		1.92	1.91
Ti	0.00	0.00	0.00	0.00	0.00	0.00	0.00	0.00	0.00	0.01	0.01	0.00	0.00	0.00	0.00	0.01	0.00	0.00	0.00	0.00		0.00	0.00
Al	1.96	1.96	1.94	1.92	1.94	1.94	1.95	1.95	1.95	1.94	1.95	1.92	1.93	1.93	1.95	1.92	1.93	1.92	1.93	1.92		0.31	0.33
Cr	0.00	0.00	0.01	0.00	0.00	0.00	0.00	0.00	0.00	0.00	0.00	0.00	0.00	0.00	0.00	0.00	0.00	0.00	0.00	0.00		0.00	0.00
Fe3	0.03	0.08	0.09	0.10	0.04	0.10	0.03	0.04	0.10	0.07	0.03	0.09	0.05	0.11	0.03	0.06	0.05	0.10	0.05	0.06		0.05	0.06
Fe2	1.27	1.18	1.17	1.17	1.23	1.15	1.23	1.21	1.16	1.19	1.23	1.20	1.23	1.19	1.27	1.23	1.24	1.17	1.21	1.22		0.16	0.14
Mn	0.03	0.03	0.03	0.03	0.03	0.03	0.03	0.03	0.04	0.04	0.04	0.04	0.04	0.04	0.03	0.03	0.03	0.03	0.02	0.03		0.00	0.00
Mg	1.13	1.18	1.19	1.21	1.15	1.17	1.15	1.15	1.12	1.13	1.09	1.13	1.14	1.18	1.12	1.16	1.17	1.20	1.20	1.18		0.60	0.60
Ca	0.57	0.59	0.58	0.57	0.60	0.62	0.60	0.62	0.64	0.63	0.65	0.63	0.61	0.56	0.58	0.59	0.57	0.58	0.58	0.58		0.74	0.72
Na	0.01	0.00	0.00	0.01	0.01	0.00	0.00	0.00	0.00	0.00	0.00	0.00	0.00	0.01	0.00	0.00	0.00	0.00	0.00	0.00		0.21	0.23
K	0.00	0.00	0.00	0.00	0.00	0.00	0.00	0.00	0.00	0.00	0.00	0.00	0.00	0.00	0.00	0.00	0.00	0.00	0.00	0.00		0.00	0.00
(mole fraction)																							
Alm	0.42	0.40	0.39	0.39	0.41	0.39	0.41	0.40	0.39	0.40	0.41	0.40	0.41	0.40	0.42	0.41	0.41	0.39	0.40	0.41 JJ	J(O)	21	23
Sps	0.01	0.01	0.01	0.01	0.01	0.01	0.01	0.01	0.01	0.01	0.01	0.01	0.01	0.01	0.01	0.01	0.01	0.01	0.01	0.01			
Prp	0.38	0.40	0.40	0.41	0.38	0.39	0.38	0.38	0.38	0.38	0.36	0.38	0.38	0.40	0.37	0.39	0.39	0.40	0.40	0.39			
Grs	0.19	0.20	0.20	0.19	0.20	0.21	0.20	0.21	0.22	0.21	0.22	0.21	0.20	0.19	0.19	0.19	0.19	0.20	0.19	0.19			

bdl = below detection limit

Table 4
Lu—Hf isotope data for Gridino-type eclogites.

Sample	Lu(ppm)	Hf(ppm)	$^{176}Lu/^{177}Hf$	$^{176}Hf/^{177}Hf$	$2\sigma_m$
Gd 07					
WR	0.3971	0.7242	0.0779	0.284778	0.000007
Grt	0.9012	0.2032	0.6330	0.306630	0.000011
Omp	0.0323	0.7772	0.0059	0.281834	0.000007
Gd 10					
WR	0.2114	0.5755	0.0522	0.283542	0.000010
Grt	0.6825	0.1317	0.7401	0.309188	0.000012
Omp	0.0318	0.6652	0.0068	0.281890	0.000008
Gd 19					
WR	0.1124	0.3444	0.0464	0.283095	0.000008
Grt	0.5023	0.1121	0.6391	0.304512	0.000013
Ky	0.0028	0.2145	0.0018	0.281195	0.000007
Gd 32					
WR	0.3261	0.6759	0.0686	0.284247	0.000006
Grt	0.7144	0.3651	0.2785	0.291654	0.000006
Omp	0.0216	0.8322	0.0037	0.281863	0.000006

NaO = 2.43, TiO_2 = 0.54, Fe_2O_3 = 0.52 in mol%, calculated from the major oxide composition of sample Gd 10 that was determined using XRF (Yu et al., 2017).

The P-T exploration window was restricted to 550–850 °C and 10–30 kbar. The composition of garnet core used for modeling was SiO_2 = 38.693 (wt%), Al_2O_3 = 21.046 (wt%), CaO = 11.452 (wt%), MgO = 6.010 (wt%), FeO = 21.106 (wt%), NaO = 0.011 (wt%), TiO_2 = 0.065 (wt%), and the compositions of garnet rim was SiO_2 = 38.780 (wt%), Al_2O_3 = 21.214 (wt%), CaO = 9.467 (wt%), MgO = 6.451 (wt%), FeO = 22.595 (wt%), NaO = 0.011 (wt%), TiO_2 = 0.044 (wt%). The P-T results for garnet core and rim are shown in Fig. 9. The optimal P-T conditions recorded by garnet are 655 °C and 18 kbar for the core (stage 1), and 660 °C and 21 kbar for the rim (stage 2). The error bars shown in Fig. 9 represent the uncertainty on the P-T estimate related to the uncertainty of the EPMA analyses, and the topology of garnet isopleths that are controlled by each reactive bulk composition.

A P-T equilibrium phase diagram calculated in the system NCFMASHTO (NaO-CaO-FeO-MgO-Al_2O_3-SiO_2-H_2O-TiO_2-Fe_2O_3) using THERMOCALC 3.33 (Powell et al., 1998; updated October 2009) was used to constrain the P-T conditions recorded by the peak mineral assemblage of sample Gd 10 (Fig. 10a, modified from Yu et al. (2017)). The activity-composition relations and the bulk compositions used in the calculation are given above. The peak mineral assemblage is interpreted to be garnet+omphacite+kyanite+rutile±quartz, in which the maximum value of J_O in omphacite ($(Na)_{M2}$ in clinopyroxene, ~ 32 mol%, see representative omphacite compositions in Yu et al.

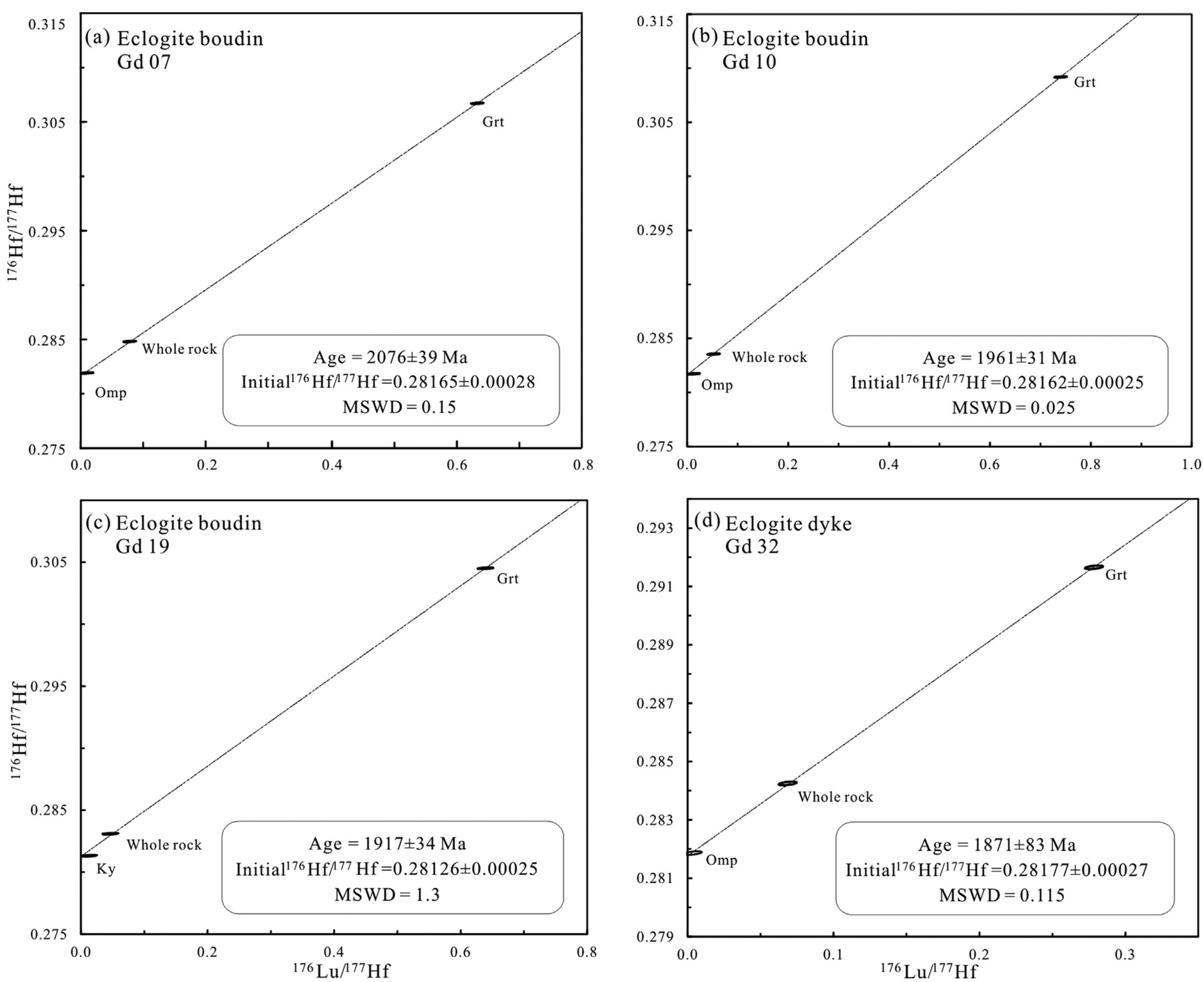

Fig. 7. Lu—Hf isochron diagrams for four Gridino-type eclogites.

Table 5
Zircon Lu—Hf isotopic data acquired by MC-LA-ICPMS.

spot		$^{176}Lu/^{177}Hf$	$^{176}Hf/^{177}Hf$	σ	Age (Ma)	σ	$^{176}Hf/^{177}Hfi$	εHf(0)	εHf(t)	s	TDM (Ma)	σ	$(^{176}Hf/^{177}Hf)DM,t$
Sample Gd 07													
Gd07-1	core	0.000394	0.281084	0.000020	2656.6	10.6	0.281064	−59.7	−0.8	0.7	2972	54	0.2813
Gd07-2	core	0.000304	0.281090	0.000017	2722.3	8.7	0.281074	−59.5	1.1	0.6	2957	44	0.2813
Gd07-3	core	0.000215	0.281118	0.000014	2669.5	9.2	0.281107	−58.5	1.1	0.5	2913	37	0.2813
Gd07-4	core	0.000286	0.281093	0.000015	2693.0	25.3	0.281078	−59.4	0.6	0.5	2952	40	0.2813
Gd07-5	core	0.000124	0.281085	0.000015	2724.1	6.7	0.281079	−59.7	1.3	0.5	2950	39	0.2812
Gd07-6	core	0.000118	0.281097	0.000013	2640.4	11.3	0.281091	−59.2	−0.2	0.5	2934	34	0.2813
Gd07-7	core	0.000352	0.281169	0.000014	2658.0	6.2	0.281151	−56.7	2.4	0.5	2855	38	0.2813
Gd07-8	core	0.000177	0.281103	0.000016	2671.0	32.0	0.281094	−59.0	0.6	0.5	2930	42	0.2813
Gd07-9	core	0.000233	0.281100	0.000016	2681.0	16.0	0.281088	−59.1	0.6	0.5	2938	42	0.2813
Gd07-10	core	0.000433	0.281131	0.000027	2696.0	37.0	0.281109	−58.0	1.7	0.9	2912	72	0.2813
Gd07-11	core	0.000316	0.281121	0.000016	2618.0	31.0	0.281105	−58.4	−0.2	0.6	2917	44	0.2813
Gd07-12	core	0.000017	0.281118	0.000017	2718.0	15.0	0.281117	−58.5	2.5	0.6	2899	45	0.2813
Gd07-13	core	0.000439	0.281123	0.000025	2705.0	15.0	0.281100	−58.3	1.6	0.9	2923	67	0.2813
Gd07-14	core	0.000347	0.281135	0.000017	2739.0	17.0	0.281117	−57.9	3.0	0.6	2900	44	0.2812
Gd07-15	core	0.000457	0.281117	0.000017	2629.0	19.0	0.281094	−58.5	−0.3	0.6	2933	46	0.2813
Gd07-16	core	0.000036	0.281071	0.000019	2687.0	19.0	0.281069	−60.2	0.1	0.7	2962	51	0.2813
Gd07-17	core	0.000338	0.281121	0.000016	2626.0	17.0	0.281104	−58.4	−0.1	0.6	2918	44	0.2813
Gd07-18	core	0.000432	0.281099	0.000013	2684.0	14.0	0.281077	−59.2	0.3	0.5	2955	36	0.2813
Gd07-19	core	0.000087	0.281153	0.000018	2701.0	16.0	0.281149	−57.3	3.3	0.6	2857	49	0.2813
Gd07-20	core	0.000070	0.281089	0.000013	2602.0	19.0	0.281086	−59.5	−1.3	0.4	2941	34	0.2813
Gd07-21	rim	0.000013	0.281572	0.000017	1915.9	7.5	0.281572	−42.4	0.3	0.6			
Gd07-22	rim	0.000016	0.281600	0.000014	1893.6	7.1	0.281599	−41.4	0.7	0.5			
Gd07-23	rim	0.000012	0.281583	0.000015	1900.6	9.4	0.281583	−42.0	0.3	0.5			
Gd07-24	rim	0.000015	0.281408	0.00003	1896.8	10.0	0.281407	−48.2	−6.0	1.0			
Gd07-25	rim	0.000010	0.281515	0.000016	1903.0	12.3	0.281515	−44.5	−2.1	0.5			
Gd07-26	rim	0.000002	0.281290	0.000047	1922.9	11.0	0.281290	−52.4	−9.6	1.6			
Gd07-27	rim	0.000006	0.281388	0.000025	1918.2	12.9	0.281388	−48.9	−6.2	0.9			
Gd07-28	rim	0.000004	0.281372	0.000018	1903.0	9.0	0.281372	−49.5	−7.1	0.6			
Gd07-29	rim	0.000006	0.281474	0.000015	1898.4	11.1	0.281474	−45.9	−3.6	0.5			
Gd07-30	rim	0.000010	0.281641	0.000014	1900.6	6.6	0.281641	−40.0	2.4	0.5			
Gd07-31	rim	0.000019	0.281580	0.000012	1906.1	7.9	0.281579	−42.2	0.3	0.4			
Gd07-32	rim	0.000013	0.281565	0.000012	1908.4	6.8	0.281565	−42.7	−0.2	0.4			
Gd07-33	rim	0.000003	0.281440	0.000037	1919.5	10.9	0.281440	−47.1	−4.3	1.3			
Gd07-34	rim	0.000004	0.281439	0.000017	1923.7	9.3	0.281439	−47.1	−4.3	0.6			
Gd07-35	rim	0.000003	0.281551	0.000013	1895.2	9.4	0.281551	−43.2	−0.9	0.5			
Sample Gd 10													
Gd10-1	rim	0.000009	0.281520	0.000015	1894.1	11.8	0.281520	−44.3	−2.1	0.5			
Gd10-2	rim	0.000007	0.281432	0.000014	1913.6	11.8	0.281432	−47.4	−4.8	0.5			
Gd10-3	rim	0.000003	0.281468	0.000019	1912.2	12.8	0.281468	−46.1	−3.5	0.7			
Gd10-4	rim	0.000007	0.281572	0.000011	1895.1	7.3	0.281572	−42.4	−0.2	0.4			
Gd10-5	rim	0.000002	0.281140	0.000087	1904.4	12.1	0.281140	−57.7	−15.3	3.0			
Gd10-6	rim	0.000023	0.281301	0.000011	1905.7	13.3	0.281300	−52.0	−9.6	0.4			
Gd10-7	rim	0.000002	0.281220	0.000063	1899.3	11.7	0.281220	−54.9	−12.6	2.2			
Gd10-8	rim	0.000012	0.281361	0.000011	1887.2	13.2	0.281361	−49.9	−7.9	0.4			
Gd10-9	rim	0.000004	0.281460	0.000019	1906.6	10.4	0.281460	−46.4	−3.9	0.7			
Gd10-10	rim	0.000006	0.281489	0.000013	1886.4	9.9	0.281489	−45.4	−3.4	0.4			
Gd10-11	rim	0.000003	0.281340	0.000053	1915.1	12.5	0.281340	−50.6	−8.0	1.9			

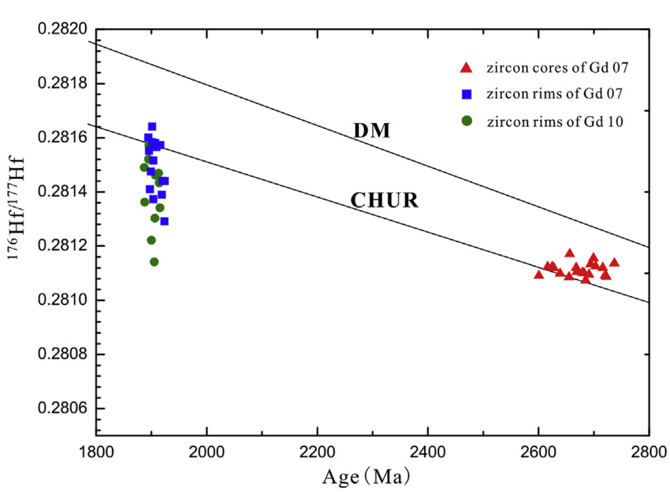

Fig. 8. Plot of U—Pb ages vs. $^{176}Hf/^{177}Hf$ ratios for zircon cores and rims from two eclogite samples. Note that the low $^{176}Hf/^{177}Hf$ zircon cores are only present in sample Gd 07.

(2017)) constrains the minimum peak pressure of 18–24 kbar (Yu et al., 2017). The occurrence of rutile inclusion in metamorphic zircon rims and the predicted paragenesis of rutile, garnet and omphacite by phase equilibria modeling indicate that rutile is one of the peak minerals (Yu et al., 2017). Zr content in rutile are 428–607 ppm (Table 6). Zr-in-rutile thermometry (Tomkins et al., 2007) for sample Gd 10 yields temperatures of 725–750 °C at 18–20 kbar, as constrained by the value of J_O 32 (Fig. 10a, stage 3). Therefore, the peak P-T conditions are proposed to be 725–750 °C at above 18 kbar on the basis of Zr-in-rutile thermometry and the maximum value of J_O (~ 32 mol%) in omphacite.

To constrain the decompression process recorded by diopside+plagioclase symplectite and paragenetic hornblende in sample Gd 10, a P-T equilibrium phase diagram was calculated in the system NCFMASH (NaO-CaO-FeO-MgO-Al_2O_3-SiO_2-H_2O) using THERMOCALC 3.33 (Powell et al., 1998; updated October 2009) with the local bulk compositions of the symplectite domain that was extracted from the compositional maps using XMapTools (Lanari and Engi, 2017). The local bulk compositions used in the calculation in mol% is: SiO_2 = 54.36, Al_2O_3 = 5.23, CaO = 17.88, MgO = 14.69, FeO = 5.08, NaO = 2.75. The phase diagram shown in Fig. 10b is contoured with isopleths of J_O. The observed mineral assemblage is diopside+plagioclase+hornblende,

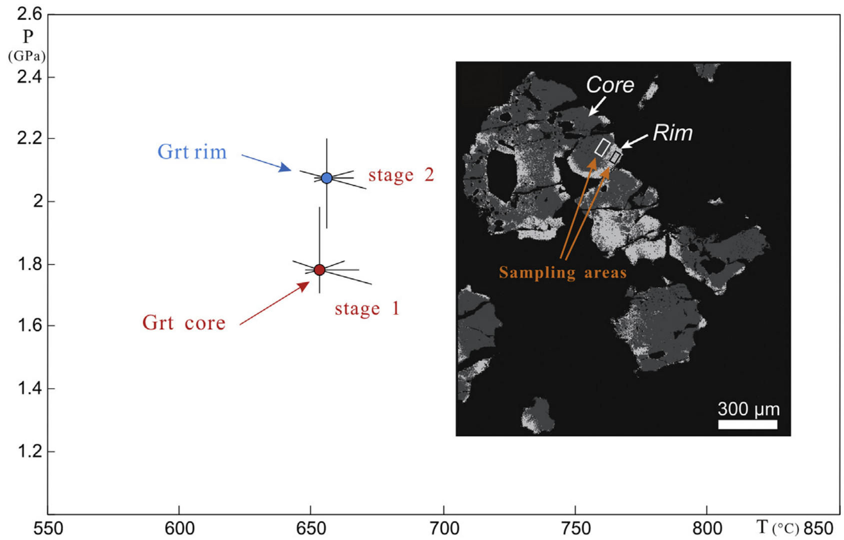

Fig. 9. P-T conditions recorded by garnet core (stage 1, 655 °C and 18 kbar) and garnet rim (stage 2, 660 °C and 21 kbar) of sample Gd 10, obtained using $G_{RT}M_{OD}$. The lines that intersect at the calculated P-T points are errors bars. X-ray map is from Fig. 3c, showing garnet cores and rims.

without quartz, which limits the maximum pressure to 9–10 kbar. The measured value of J_O (about 9 mol%, Table 2) in diopside constrains similar maximum pressure (9–10 kbar) in the Di-Pl-Hbl field. The amphibole–plagioclase thermometer (Holland and Blundy, 1994) yield a temperature range of 680–730 °C at 9–10 kbar for hornblende and plagioclase grains located in the symplectite (Fig. 10b, stage 4; representative mineral compositions are listed in Table 2). These conditions are interpreted to represent the P-T conditions of the retrograde high-pressure granulite facies metamorphism.

7. Discussion

7.1. P-T path of the Gridino-type eclogite

Garnet porphyroblasts in eclogite sample Gd 10 have large homogeneous cores and thin rims. The garnet shows relatively flat compositional profiles. This suggests two possible scenarios should be considered: (1) The garnet cores may have undergone very rapid growth, thus the initial compositional profiles are flat (Carlson, 2006; Florence and Spear, 1991). In this scenario, the calculated P-T conditions for garnet cores and rims can be interpreted as growth conditions, defining an up pressure growth from core to rim (Fig. 11a, stage 1 to stage 2). (2) The sample has reached peak temperature of above 700 °C (based on Zr-in-rutile T), and an alternative scenario is that diffusion affected the compositional zoning of the garnet core compositions resulting in the homogenization of the composition before the growth of the rim (see below). Thus, the P-T conditions recorded by garnet cores would represent re-equilibration conditions rather than growth conditions (Tedeschi et al., 2017). The sharp compositional transition observed between core and rim (Fig. 3f) suggest that diffusion was limited after the growth of garnet rim. The composition of garnet rim was therefore not affected by diffusion and is likely to reflect growth conditions. The observed compositional trend (stage 1 to stage 2) also suggests an up-pressure path from garnet core to rim. Considering that the composition of garnet has been modified around amphibole inclusion (Fig. 3), we favor scenario (2): diffusion homogenized the

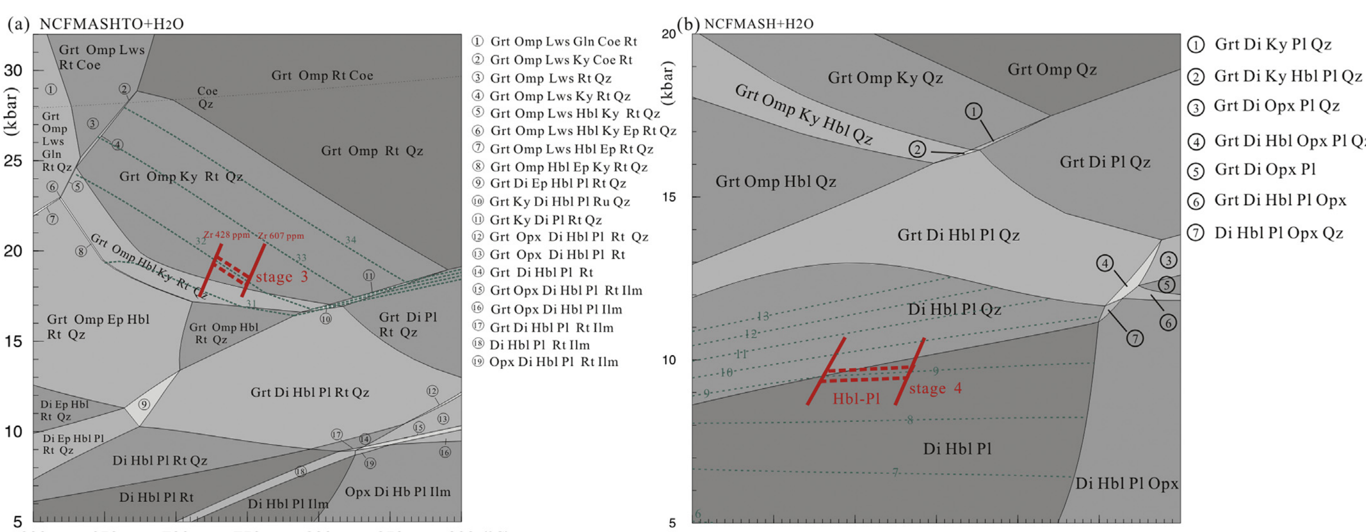

Fig. 10. (a) Pseudosection for the peak area of sample Gd 10, modified after Yu et al. (2017). The temperatures range from Zr-in-rutile thermometry is shown by the red bar. Isopleths of J_O ($(Na)_{M2}$ in clinopyroxene) are in green; (b) Pseudosection for the retrograde stage of sample Gd 10. Constraints from Hbl-Pl thermometery are indicated by the red bars. Isopleths of J_O ($(Na)_{M2}$ in clinopyroxene) are in green. (For interpretation of the references to color in this figure legend, the reader is referred to the web version of this article.) (For interpretation of the references to color in this figure legend, the reader is referred to the web version of this article.)

Table 6
Zr content in rutiles of sample Gd 10.

Samples	Gd10–1	Gd10–2	Gd10–3	Gd10–4	Gd10–5	Gd10–6	Gd10–7	Gd10–8	Gd10–9	Gd10–10	Gd10–11	Gd10–12
Zr(ppm)	509	521	539	607	482	428	465	435	588	553	553	446
ln(Zr)	6.23	6.26	6.29	6.41	6.18	6.06	6.14	6.08	6.38	6.32	6.32	6.10
P	18	18	18	18	18	18	18	18	18	18	18	18
T	735	737	740	751	730	720	727	721	748	742	742	723
P	22	22	22	22	22	22	22	22	22	22	22	22
T	755	757	760	771	750	739	747	741	768	763	763	743

Zr-in-rutile thermometry from Tomkins et al., 2007

composition of garnet cores at ~655 °C and ~18 kbar, before the growth of the garnet rim. Garnet rims formed later on (Fig. 11a, stage 2) closer to the pressure peak conditions (Fig. 11a, stage 3) with limited post-growth modification by diffusion. Garnet reflecting higher-pressure conditions may also have formed but it was probably consumed during retrograde metamorphism (Groppo et al., 2015; O'Brien, 1997); garnet porphyroblasts are not euhedral (Figs. 2 and 3) and Mn zoning (Mn back diffusion; Fig. 3f) clearly suggests garnet resorption during retrogression.

In previous studies of Gridino-type eclogite, garnet has always been used to constrain the peak P-T conditions and P-T paths (e.g. Li et al., 2015; Perchuk and Morgunova, 2014; Yu et al., 2017, Fig. 11b). As discussed above, the compositions of the garnet cores may have been modified by diffusion. Thus, care is needed while using garnet composition to constrain P-T conditions. Rutile is another peak mineral of sample Gd 10. Zr-in-rutile thermometry is robust technique. Applying phase equilibrium modeling and Zr-in-rutile thermometry can reduce drastically the uncertainties of the calculated P-T conditions (Hernández-Uribe et al., 2018), which constrains the peak P-T conditions at 725–750 °C, above 18 kbar (Fig. 11a, stage 3). Similar peak P-T conditions of the Gridino-type eclogite have been reported: 700–730 °C, 18.5–19.5 kbar (Li et al., 2015) or 695–755 °C, >18 kbar (Yu et al., 2017), and in both cases the peak temperature was constrained by the garnet-clinopyroxene thermometer. Considering that diffusion may affect the compositional zoning of garnets and the rare preservation of garnet compositions reflecting peak conditions in the Gridino-type eclogites, the peak conditions obtained with garnet may be unreliable. In this study we provided an alternative and more robust approach in an attempt to constrain minimum peak conditions (Hernández-Uribe et al., 2018).

The high-pressure granulite facies overprinting occurred during the subsequent exhumation stage, leading to the breakdown of omphacite to clinopyroxene, plagioclase and amphibole. Symplectite textures commonly indicate a departure from efficient equalization of chemical potentials. However, the absence of clear layering in the final chemical compositions (e.g. Fig. 4) suggests that chemical potential gradients were close to be equalized by diffusion (White et al., 2001). The final composition of the microstructure was taken as natural variable for modeling the equilibrium relationships. This assumption is also supported by the modes predicted by our modeling at 710 °C and 9 kbar that reasonably match the volume fractions extracted from the map assuming absolute uncertainties of ±0.05 (molar proportion normalized to a one oxide basis) for the model and ± 0.05 vol% from the phase map. Combined with this result, the amphibole-plagioclase thermometer (Holland and Blundy, 1994) defines a stage at 680–730 °C at 9–10 kbar (Fig. 11a, stage 4), corresponding to the P-T conditions of the high-pressure granulite facies metamorphism. A heating stage up to 800 °C at 12 kbar has been previously proposed on the basis of the mineral assemblage Grt + Cpx + Opx + Pl + Qz in some samples (Morgunova and Perchuk, 2012). No orthopyroxene was found in our samples or samples in Li et al. (2015) and Yu et al. (2017).

Garnet core and rim testify a burial process that corroborates the prograde path inferred by mineral inclusions preserved in garnet cores (Yu et al., 2017). P-T conditions retrieved from symplectites indicate a cooling decompression. Thus, we propose a clockwise metamorphic evolution for the Gridino-type eclogites.

7.2. Lu—Hf age interpretation

It is not always straightforward to link garnet Lu—Hf ages with a specific garnet growth stage and their corresponding P-T conditions. Garnet Lu—Hf ages in the Gridino samples are obtained from bulk garnet aliquots of grains that present weak major element zoning. In sample Gd 10, the large weakly zoned garnet cores may be the product of high temperature diffusional re-equilibration of major elements.

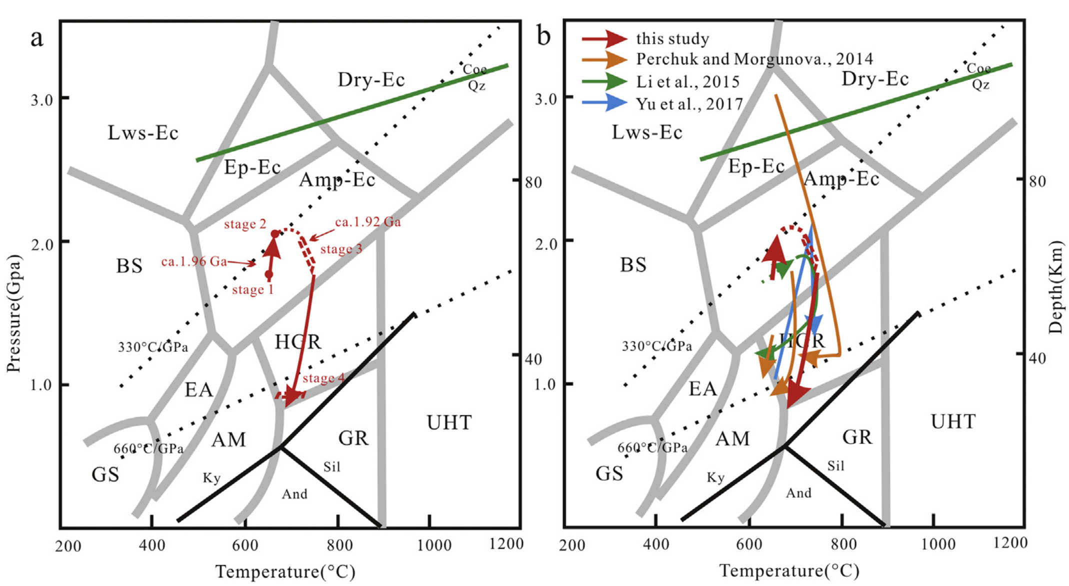

Fig. 11. Inferred P-T-t path for metamorphic evolution of Gridino-type eclogite: (a) with metamorphic age; (b) with other inferred P-T paths.

However, diffusion of major elements may or may not be coupled with resetting of Lu—Hf (Scherer et al., 2000; Smit et al., 2013). The closure temperature of the garnet Lu—Hf system, is determined by various factors such as grain size and cooling rates (Dodson, 1973). The peak temperature of Gridino-type eclogite are constrained below 755 °C (Li et al., 2015; Yu et al., 2017; this study), which is lower than the excepted closure temperature of the garnet Lu—Hf system (>900–1000 °C) (Dodson, 1973; Scherer et al., 2000; Smit et al., 2013). Given that 3+ and 4+ ions (Lu, Hf) diffuse significantly slower than 2+ ions (Mg, Mn) in garnet (Tirone et al., 2005; Van Orman et al., 2002), Lu and Hf probably maintain their original distributions in Gd 10 garnet. Therefore, we interpreted the obtained Lu—Hf ages for the large size garnet from Gridino-type eclogite samples as garnet growth ages rather than cooling ages.

Element-mapping shows large cores and thin rims of garnet in sample Gd 10, with limited compositional zoning in cores (Yu et al., 2017; this study). The calculated P-T conditions indicate an increase in pressure from garnet core to rim. The garnet Lu—Hf age for sample Gd 10 is closer to the age of the garnet cores since the garnet core is the main part of the single garnet grain and Lu is commonly enriched in prograde garnet cores (Scherer et al., 2000). Therefore, we interpret the Lu—Hf age of 1961 ± 31 Ma to record the prograde garnet growth stage (Fig. 11a). The eclogite sample Gd 07 shares with sample Gd 10 similar petrography and mineral chemistry, without compositional zoning in garnet (Yu et al., 2017). Despite these similarities, the obtained Lu—Hf garnet ages for sample Gd 07 and sample Gd 10 are not the same within uncertainty and Gd 07 returns an older age. This discrepancy can be explained considering the different zircon populations in the two samples. In sample Gd 07, the inherited magmatic zircon cores are abundant and well preserved (Yu et al., 2017). These zircon cores have $^{176}Hf/^{177}Hf$ ratios of 0.281071–0.281169, much lower than the $^{176}Hf/^{177}Hf$ ratios of the corresponding whole rock (0.284788) and garnet (0.306630). The inherited zircon cores are not in isotopic equilibrium with the bulk rock and the metamorphic assemblage including garnet, and any contamination from zircon in the garnet aliquot would produce an apparent garnet Lu—Hf age that is too old (Cheng et al., 2008, 2012; Scherer et al., 2000). Therefore, we suggest that the Lu—Hf ages for sample Gd 07 of 2076 ± 39 Ma is older because of contamination from inherited zircon cores in garnet of sample Gd 07.

Most garnet grains in sample Gd 19 preserve weak compositional zoning (Fig. 6). Only in the outmost rims does some grains display a slight decrease in pyrope and grossular, and increase in almandine. Garnet is larger in sample Gd 19 than that in Gd 10. Theoretically diffusion of Lu and Hf will take longer time. Lu and Hf should also maintain their original distribution in Gd 19 garnet. Thus, the obtained Lu—Hf age of 1917 ± 34 Ma for sample Gd 19 is similarly interpreted as dating a prograde P-T stage. The Lu—Hf age variation between sample Gd 10 and Gd 19 is more likely to reflect either variable REE zoing between the two samples or the uncertainty of age that is amplified by the reliance on just one garnet separate. The obtained Lu—Hf age 1871 ± 83 Ma for sample Gd 32 is within uncertainty the same as the other eclogite samples. The minerals grain size in sample Gd 32 (0.3–0.6 mm) is smaller than in the other samples (Yu et al., 2017), likely resulting in a lower closure temperature for the Lu—Hf system (Dodson, 1973). The variable preservation of growth Lu and Hf distribution in garnet grains could be the reason for the relatively large uncertainty of the Lu—Hf age from this sample.

In summary, the age of 1961 ± 31 Ma constrains the prograde stage of Gridino-type eclogite. The 1917 ± 34 Ma age also represents a prepeak stage, which is within the uncertainty similar to the metamorphic zircon ages of 1904.2 ± 4.1 Ma and 1898.6 ± 5.3 Ma for Gridino-type eclogite (Yu et al., 2017). These metamorphic zircon rims show trace element systematics characteristic of eclogite-facies metamorphism and contain the peak mineral inclusions, garnet and omphacite (Yu et al., 2017). Yu et al. (2017) demonstrated that the REE partition coefficients between zircon rim and garnet are consistent with values of typical eclogites. These lines of evidence suggest that the metamorphic zircon rims in Gridino-type eclogite formed during eclogite facies metamorphism.

Table 7
A compilation of peak metamorphic ages for the Belomorian eclogites.

	Gridino-type	Salma-type
Zircon U-Pb	1904 ± 4 Ma (Yu et al., 2017); 1880 Ma (Skublov et al., 2011a)	1911 ± 6 Ma (Li et al., 2017a); 1896 Ma-1885 ± 7 Ma (Liu et al., 2017); 1868 ± 17 Ma (Imayama et al., 2017)
Grt Lu-Hf	1917 ± 34 Ma (this study); 1937 ± 8 Ma-1891 ± 10 Ma (Herwartz et al., 2012)	1901 ± 5 Ma-1894 ± 4 Ma (Herwartz et al., 2012)
Grt Sm-Nd	1911 ± 11 Ma (Berezin et al., 2012)	

A compilation of peak metamorphic ages for the Gridino- and Salma-type eclogites is presented in Table 7. Our new garnet ages and P-T path can help interpret prior Lu—Hf garnet ages of 1937.3 ± 8.2 Ma and 1891.6 ± 9.7 Ma for the Gridino-type eclogites obtained by Herwartz et al. (2012). The age of ca. 1.94 Ga can be regarded as the prograde garnet growth episode, while the younger age of ca. 1.89 Ga is close to the peak age. The adjacent Salma-type eclogites have also been proven to be Paleoproterozoic using zircon geochronology and garnet Lu—Hf geochronology (Herwartz et al., 2012; Imayama et al., 2017; Li et al., 2017a, 2017b; Liu et al., 2017).

7.3. Geological implications

It has been proposed that the protolith of Gridino-type eclogite formed at ca. 2.7 Ga from an enriched mantle source (Mints et al., 2014; Skublov et al., 2011a, 2011b; Yu et al., 2017). After several thermal and deformation pulses from Neoarchean to Paleoproterozoic (Babarina and Sibelev, 2015; Mints et al., 2014), the Lapland-Kola orogen recorded eclogite-facies metamorphism at ca. 1.9 Ga leading to the formation of Gridino-type eclogites (Yu et al., 2017).

Paleoproterozoic eclogites are preserved in the Trans-Hudson Orogeny in Canada (Weller and St-Onge, 2017), Trans-North China Orogeny (Xu et al., 2017), Snowbird Craton in Canada (Baldwin et al., 2007), Slave eclogite xenolith in Canada (Smart et al., 2014, 2016), Usagaran and Ubendian Orogeny in Tanzania (Boniface et al., 2012; Collins et al., 2004), Eburnian-Transamazonian Orogen in southern Cemeroon (Loose and Schenk, 2018) and the Belomorian Province in Russia (this study). These Paleoproterozoic eclogites are located within collisional orogens that mark the assembly of the supercontinent Columbia at 2.1–1.8 Ga (Zhao et al., 2002).

Among them, the Belomorian and Trans-Hudson eclogites have low peak metamorphic thermal gradients (Weller and St-Onge, 2017; this study), which are typical characteristics of Phanerozoic eclogites (Brown, 2006; Maruyama et al., 1996). It has to be noted that, unlike the Belomorian eclogites, no direct dating of the eclogitic assemblage has been achieved for the Trans-Hudson retrogressed eclogites, whose age constraint is based on monazite dating of the surrounding metapelites (Weller and St-Onge, 2017). Thus, the Belomorian eclogites are the best-dated Paleoproterozoic cold-eclogites. Moreover, the contemporaneous ultra-high-temperature metamorphism recorded in the Ouzaal Terrain in Algeria, Taltson magmatic zone in Canada and South Harris in Scotland indicates the duality of the thermal regime in this period (Brown, 2006; Brown, 2007; Brown, 2008), thus strengthening the conclusion that the Paleoproterozoic marks the start for modern plate tectonics on a global scale.

8. Conclusions

(1) New garnet Lu—Hf geochronology constrains the prograde stage of Gridino-type eclogite at ca. 1.96–1.92 Ga.
(2) The peak pressure conditions are 725–730 °C at above 18 kbar, and define an average apparent thermal gradient of below 41 °C/kbar.
(3) The metamorphic evolution of Gridino-type eclogite follows a clockwise P-T paths with a cooling decompression from peak eclogite facies to high-pressure granulite facies.

Acknowledgments

We thank Yueheng Yang (State Key Laboratory of Lithospheric Evolution, Institute of Geology and Geophysics CAS) for his help in garnet Lu—Hf geochronology. We also thank the reviewers for their great comments and suggestions. This work was supported by National Nature Science Foundation of China [Grant 41121062, 41172196 and 41311120071].

References

Anczkiewicz, R., Thirlwall, M.F., 2003. Improving Precision of Sm-Nd Garnet Dating by H_2SO_4 Leaching: A Simple Solution to the Phosphate Inclusion Problem. vol. 220. Geological Society, London, Special Publications, pp. 83–91.
Babarina, I.I., Sibelev, O.S., 2015. Deformation events in the Gridino zone, Belomorian Province, Fennoscandian Shield: relationships between mafic dike swarms and eclogite-bearing mélange. International Geology Review 57, 1607–1618.
Balagansky, V.V., 2002. Main Stages of the Paleoproterozoic Tectonic Evolution of the Northeastern Baltic Shield. Doctoral Dissertation. vol. 326. Russian Academy of Sciences (In Russian).
Baldwin, J.A., Powell, R., Williams, M.L., Goncalves, P., 2007. Formation of eclogite, and reaction during exhumation to mid-crustal levels, Snowbird tectonic zone, western Canadian Shield. Journal of Metamorphic Geology 25, 953–974.
Berezin, A.V., Travin, V.V., Marin, Y.B., Skublov, S.G., Bogomolov, E.S., 2012. New U-Pb and Sm-Nd ages and P-T estimates for eclogitization in the Fe-rich gabbro dyke in Gridino area (Belomorian mobile belt). Doklady Earth Sciences 444, 760–765.
Bibikova, E., Skiöld, T., Bogdanova, S., Gorbatschev, R., Slabunov, A., 2001. Titanite–rutile thermochronometry across the boundry between the Archean craton in Karelia and the Belomorian mobile belts. Precambrian Research 105, 315–330.
Blichert-Toft, J., Chauvel, C., Albarede, F., 1997. Separation of Hf and Lu for high-precision isotope analysis of rock samples by magnetic sector-multiple collector ICP-MS. Contributions to Mineralogy and Petrology 127, 248–260.
Boniface, N., Schenk, V., Appel, P., 2012. Paleoproterozoic eclogites of MORB-type chemistry and three Proterozoic orogenic cycles in the Ubendian Belt (Tanzania): Evidence from monazite and zircon geochronology, and geochemistry. Precambrian Research 192–195, 16–33.
Brown, M., 2006. Duality of thermal regimes is the distinctive characteristic of plate tectonics since the Neoarchean. Geology 34, 961–964.
Brown, M., 2007. Metamorphic conditions in orogenic belts: a record of secular change. International Geology Review 49, 193–234.
Brown, M., 2008. Characteristic Thermal Regimes of Plate Tectonics and their Metamorphic Imprint throughout Earth History: When Did Earth First Adopt a Plate Tectonics Mode of Behavior? The Geological Society of America, pp. 97–128 Special paper 440
Brown, M., 2014. The contribution of metamorphic petrology to understanding lithosphere evolution and geodynamics. Geoscience Frontiers 5, 553–569.
Carlson, W.D., 2006. Rates of Fe, Mg, Mn, and Ca diffusion in garnet. American Mineralogist 91, 1–11.
Carswell, D.A., 1990. Eclogites and the eclogite-facies: definitions and classification. In: Carswell, D.A. (Ed.), Eclogite-facies Rocks. Glasgow, Blackie, pp. 1–13.
Cheng, H., King, R.L., Nakamura, E., Vervoort, J.D., Zhou, Z., 2008. Coupled Lu-Hf and Sm-Nd geochronology constrains garnet growth in ultra-high-pressure eclogites from the Dabie orogen. Journal of Metamorphic Geology 26, 741–758.
Cheng, H., Zhang, C., Vervoort, J.D., Li, X.H., Li, Q.L., Wu, Y.B., Zheng, S., 2012. Timing of eclogite facies metamorphism in the North Qinling by U-Pb and Lu-Hf geochronology. Lithos 136 (139), 46–59.
Cheng, H., Liu, Y.M., Vervoort, J.D., Lu, H.H., 2015. Combined U-Pb, Lu-Hf, Sm-Nd and Ar-Ar multichronometric dating on Bailang eclogite constrains the closure timing of the Paleo-Tethys Ocean in the Lhasa terrane, Tibet. Gondwana Research 28, 1482–1499.
Collins, A.S., Reddy, S.M., Buchan, C., Mruma, A., 2004. Temporal constraints on Palaeoproterozoic eclogite formation and exhumation (Usagaran Orogen, Tanzania). Earth and Planetary Science Letters 224, 175–192.
Condie, K.C., Kröner, A., 2008. When Did Plate Tectonics Begin? Evidence from the Geologic Record. The Geological Society of America, pp. 281–294 Special paper 440.
Daly, J.S., Balagansky, V.V., Timmerman, M.J., Whitehouse, M.J., 2006. The Lapland-Kola orogen: Palaeoproterozoic collision and accretion of the northern Fennoscandian lithosphere. The Geological Society of London 32, 579–598.
Diener, J.F.A., Powell, R., White, R.W., Holland, T.J.B., 2007. A new thermodynamic model for clino-and orthoamphiboles in the system $Na_2O–CaO–FeO–MgO–Al_2O_3–SiO_2–H_2O–O$. Journal of Metamorphic Geology 25, 631–656.
Dodson, M.H., 1973. Closure temperature in cooling geochronological and petrological systems. Contributions to Mineralogy and Petrology 40, 259–264.
Dokukina, K.A., Kaulina, T.V., Konilov, A.N., Mints, M.V., Lepekhina, E.N., 2014. Archean to Palaeoproterozoic high-grade evolution of the Belomorian eclogite province in the Gridino area, Fennoscandian shield: geochronological evidence. Gondwana Research 25, 585–613.
Duchêne, S., Blichert-Toft, J., Luais, B., Télouk, P., Lardeaux, J.M., Albarède, F., 1997. The Lu-Hf dating of garnets and the ages of the Alpine high-pressure metamorphism. Nature 387, 586–589.
Engi, M., Lanari, P., Kohn, M.J., 2017. Significant ages — an introduction to petrochronology. Reviews in Mineralogy and Geochemistry 83, 1–12.
Florence, F.P., Spear, F.S., 1991. Effects of diffusional modification of garnet growth zoning on P-T path calculations. Contributions to Mineralogy and Petrology 107, 487–500.
Gaidies, F., De Capitani, C., Abart, R., Schuster, R., 2008. Prograde garnet growth along complex P-T-t paths: results from numerical experiments on polyphase garnet from the Wölz complex (Austroalpine Basement). Contributions to Mineralogy and Petrology 155, 673–688.
Green, E.C.R., Holland, T.J.B., Powell, R., 2007. An order-disorder model for omphacitic pyroxenes in the system jadeite–diopside–hedenbergite–acmite, with applications to eclogitic rocks. American Mineralogist 92, 1181–1189.
Groppo, C., Rolfo, F., Liu, Y.C., Deng, L.P., Wang, A.D., 2015. P-T evolution of elusive UHP eclogites from the Luotian dome (North Dabie Zone, China): how far can the thermodynamic modeling lead us? Lithos 226, 183–200.
Hernández-Uribe, D., Mattinson, C.G., Zhang, J., 2018. Phase equilibrium modelling and implications for P-T determinations of medium-temperature UHP eclogites, North Qaidam terrane, China. Journal of Metamorphic Geology 1–25.
Herwartz, D., Skublov, S.G., Berezin, A.V., et al., 2012. First Lu-Hf garnet ages of eclogites from the Belomorian mobile belt (Baltic shield, Russia). Doklady Earth Sciences 443, 377–380.
Holland, T., Blundy, J., 1994. Non-ideal interactions in calcic amphiboles and their bearing on amphibole-plagiclase thermometry. Contributions to Mineralogy and Petrology 116, 433–447.
Holland, T.J.B., Powell, R., 1998. An internally consistent thermodynamic data set for phases of petrological interest. Journal of Metamorphic Geology 16, 309–343.
Holland, T., Powell, R., 2003. Activity-composition relations for phases in petrological calculations: an asymmetric multi-component formulation. Contributions to Mineralogy and Petrology 145, 492–501.
Hölttäs, P., Balagansky, V., Garde, A.A., et al., 2008. Archean of Greenland and Fennoscandia. Episodes 31, 13–18.
Imayama, T., Oh, C.W., Batybaev, S.K., Park, C.S., Yi, K., Jung, H., 2017. Paleoproterozoic high-pressure metamorphic history of the Salma eclogite on the Kola Peninsula, Russia. Lithosphere.
Johnson, T.E., Brown, M., Kaus, B.J.P., Vantongeren, J.A., 2014. Delamination and recycling of Archaean crust caused by gravitational instabilities. Nature Geoscience 7, 47–52.
Korikovsky, S.P., Kotov, A.B., Sal'nikova, E.B., Aranovich, L.Y., Korpechkov, D.I., Yakovleva, S.Z., Tolmacheva, E.V., 2014. The age of the protolith of Metamorphic rocks in the southeastern part of the Lapland granulite belt, southern Kola Peninsula: correlation with the Belomorian Mobile Belt in the Context of the problem of Archean eclogites. Petrology 22, 91–108.
Kylander-Clark, A.R.C., Hacker, B.R., Johnson, C.M., Beard, B., et al., 2007. Coupled Lu-Hf and Sm-Nd geochronology constrains prograde and exhumation histories of high-and ultrahigh-pressure eclogites from western Norway. Chemical Geology 242, 137–154.
Lagos, M., Scherer, E.E., Tomaschek, F., Münker, C., Keiter, M., Berndt, J., Ballhaus, C., 2007. High Precision Lu-Hf geochronology of Eocene eclogite-facies rocks from Syros, Cyclades, Greece. Chemical Geology 243, 16–35.
Lanari, P., Engi, M., 2017. Local bulk composition effects on metamorphic mineral assemblage. Reviews in Mineralogy and Geochemistry 83, 55–102.
Lanari, P., Riel, N., Guillot, S., Vidal, O., Hattori, K., 2013. Deciphering high-pressure metamorphism in collisional context using microprobe mapping methods: application to the Stak eclogitic massif (northwest Himalaya). Geology 41, 111–114.
Lanari, P., Vidal, O., De Andrade, V., Dubacq, B., Lewin, E., 2014. XMapTools: a MATLAB-based program for electron microprobe X-ray image processing and geothermobarometry. Computers & Geosciences 62, 227–240.
Lanari, P., Giuntoli, F., Loury, C., Burn, M., Engi, M., 2017. An inverse modeling approach to obtain P-T conditions of metamorphic stage involving garnet growth and resorption. European Journal of Mineralogy 29, 181–199.
Lanari, P., Vho, A., Bovay, T., Airaghi, L., Centrella, S., 2018. Quantitative Compositional Mapping of Mineral Phases by Electron Probe Micro-Analyser. Special Publication of the Geological Society of London (in press).
Lapen, T.J., Johnson, C.M., Baumgartner, L.P., Mahlen, N.J., Beard, B.L., Amato, J.M., 2003. Burial rates during prograde metamorphism of an ultra-high-pressure terrane: an example from Lago di Cignana, weatern Alps, Italy. Earth and Planetary Science Letters 215, 57–72.
Li, X.L., Zhang, L.F., Wei, C.J., Slabunov, A.I., 2015. Metamorphic PT path and zircon U–Pb dating of Archean eclogite association in Gridino complex, Belomorian province, Russia. Precambrian Research 268, 74–96.
Li, X.L., Yu, H.L., Zhang, L.F., Wei, C.J., Bader, T., 2017a. 1.9 Ga eclogite from the Archean-Paleoproterozoic Belomorian Province, Russia. Science Bulletin 62, 239–241.
Li, X.L., Zhang, L.F., Wei, C.J., Slabunov, A.I., Bader, T., 2017b. Neoarchean-Paleoproterozoic granulite-facies metamorphism in Uzkaya Salma eclogite-bearing mélange, Belomorian Province (Russia). Precambrian Research 294, 257–283.

Li, X.L., Zhang, L.F., Wei, C.J., Slabunov, A.I., Bader, T., 2017c. Quartz and orthopyroxene exsolution lamellae in clinopyroxene and the metamorphic P–T path of Belomorian eclogites. Journal of Metamorphic Geology 00, 1–22.

Liu, F.L., Zhang, L.F., Li, X.L., et al., 2017. The metamorphic evolution of Paleoproterozoic eclogites in Kuru-Vaara, northern Belomorian Province, Russia: constraints from P–T pseudosections and zircon dating. Precambrian Research 289, 31–47.

Loose, D., Schenk, V., 2018. 2.09 Ga old eclogites in the Eburnian-Transamazonian orogen of southern Cameroon: significance for Palaeoproterozoic plate tectonics. Precambrian Research 304, 1–11.

Ludwig, K.R., 2012. A Geochronological Toolkit for Microsoft Excel. vol. 5. Berkeley Geochronology Center Special Publication, pp. 1–75.

Maruyama, S., Liou, J.G., Terabayashi, M., 1996. Blueschists and eclogites of the world and their exhumation. International Geology Review 38, 485–594.

Mints, M.V., Belousova, E.A., Konilov, A.N., et al., 2010. Mesoarchean subduction processes: 2.87 Ga eclogites from the Kola Peninsula, Russia. Geology 38, 739–742.

Mints, M.V., Dokukina, K.A., Konilov, A.N., 2014. The Meso-Neoarchean Belomorian eclogite province: tectonic position and geodynamic evolution. Gondwana Research 25, 561–584.

Miyashiro, A., 1961. Evolution of metamorphic belts. Journal of Petrology 2, 277–311.

Morgunova, A.A., Perchuk, A.L., 2012. Ultrahigh-Pressure Metamorphism in the Archean-Proterozoic Mobile Belt (Gridino Complex, Karelia, Russia). vol. 443 pp. 412–416.

Mudruk, S.V., Balagansky, V.V., Gorbunov, I.A., Raevsky, A.B., 2013. Alpine-type tectonics in the Paleoproterozoic Lapland-Kola orogeny. Geotectonics 47, 251–265.

Nesterova, N.S., Kirnozova, T.I., Fugzan, M.M., 2011. New U-Pb titanite age data on the rocks from the Karelian Craton and the Belomorian Mobile Belt, Fennoscandian Shield. Geochemistry International 49, 1161–1167.

O'Brien, P.J., 1997. Garnet zoning and reaction textures in overprinted eclogites, Bohemian Massif, European Variscides: a record of their thermal history during exhumation. Lithos 41, 119–133.

Perchuk, A.L., Morgunova, A.A., 2014. Variable P-T paths and HP-UHP metamorphism in a Precambrian terrane, Gridino, Russia: Petrological evidence and geodynamic implications. Gondwana Research 25, 614–629.

Philippot, P., Blichert-Toft, J., Perchuk, A., Costa, S., Gerasimov, V., 2001. Lu-Hf and Ar-Ar chronometry supports extreme rate of subduction zone metamorphism deduced from geospeedometry. Tectonophysics 342, 23–38.

Powell, R., Holland, T., Worley, B., 1998. Calculating phase diagram involving solid solutions via non-linear equations, with examples using THERMOCALC. Journal of Metamorphic Geology 16, 577–586.

Ruchyev, A.M., 2000. On the protolith of the North Karelian gneisses of the Chupa suite, Belomorian complex. Geology and useful minerals of Karelia 2, 12–25 (In Russian).

Scherer, E.E., Cameron, K.L., Blichert-Toft, J., 2000. Lu-Hf garnet geochronology: closure temperature relative to the Sm-Nd system and the effects of trace mineral inclusions. Geochimica et Cosmochimica Acta 64, 3413–3432.

Scherer, E.E., Münker, C., Mezger, K., 2001. Calibration of the lutetium-hafnium clock. Science 293, 683–687.

Skublov, S.G., Astaf'ev, B.Y., Marin, Y.B., Berezin, A.V., Mel'nik, A.E., Presnyakov, S.L., 2011a. New data on the age of eclogites from the Belomorian mobile belt at Gridino settlement area. Doklady Earth Sciences 439, 1163–1170.

Skublov, S.G., Berezin, A.V., Mel'nik, A.E., 2011b. Paleoproterozoic Eclogites in the Salma Area, Northwestern Belomorian Mobile Belt: composition and isotopic geochronologic characteristics of minerals and metamorphic age. Doklady Earth Sciences 19, 470–495.

Skublov, S.G., Berezin, A.V., Rizvanova, N.G., Mel'nik, A.E., Myskova, T.A., 2014. Multistage Svecofennian metamorphism: evidence from the composition and U-Pb age of titanite from eclogites of the Belomorian mobile belt. Petrology 22, 381–388.

Slabunov, A.I., Lobach-Zhuchenko, S.B., Bibikova, E.V., Sorjonen-Ward, P., Balagansky, V.V., Stepanov, V.S., 2006. The Archaean nucleus of the Fennoscandian (Baltic) Shield. The Geological Society of London 32, 627–644.

Sláma, J., Košler, J., Condon, D.J., Crowley, J.L., ... Whitehouse, M.J., 2008. Plešovice zircon-a new natural reference material for U-Pb and Hf isotopic microanalysis. Chemical Geology 249, 1–35.

Smart, K.A., Chacho, T., Simonetti, A., Sharp, Z.D., Heaman, L.M., 2014. A record of Paleoproterozoic subduction preserved in the northern Slave cratonic mantle: Sr-Pb-O isotope and trace-element investigations of eclogite xenoliths from the Jericho and Muskox kimberlites. Journal of Petrology 55, 549–583.

Smart, K.A., Tappe, S., Simonetti, A., Simonetti, S.S., Woodland, A.B., Harris, C., 2016. Tectonic significance and redox state of Paleoproterozoic eclogite and pyroxenite components in the Slave cratonic mantle lithosphere, Voyageur kimberlite, Arctic Canada. Chemical Geology 455, 98–119.

Smit, M.A., Scherer, E.E., Mezger, K., 2013. Lu–Hf and Sm–Nd garnet geochronology: chronometric closure and implications for dating petrological processes. Earth and Planetary Science Letters 381, 222–233.

Spear, F.S., Selverstone, J., 1983. Quantitative P-T paths from zoned minerals: theory and tectonic applications. Contributions to Mineralogy and Petrology 83, 348–357.

Stepanova, A.V., Samsonov, A.V., Salnikova, E.B., Puchtel, I.S., Larionova, Y.O., Larionov, A. N., Stepanov, V.S., Shapovalov, Y.B., Egorova, S.V., 2014. Palaeoproterozoic continental MORB-type tholeiites in the Karelian craton: petrology, geochronology, and tectonic setting. Journal of Petrology 55, 1719–1751.

Stern, R.J., 2008. Modern-Style Plate Tectonics Began in Neoproterozoic Time: An Alternative Interpretation of Earth's Tectonic History. The Geological Society of America, pp. 265–280 Special paper 440.

Tedeschi, M., Lanari, P., Rubatto, D., Pedrosa-Soares, A., Hermann, J., Dussin, I., Pinheiro, M. A.P., Bouvier, A.S., Baumgartner, L., 2017. Reconstruction of multiple P-T-t stages from retrogressed mafic rocks: subduction versus collision in the Southern Brasília orogen (SE Brazil). Lithos 294 (295), 283–303.

Tirone, M., Ganguly, J., Dohmen, R., Langenhorst, F., Hervig, R., Becker, H.W., 2005. Rare earth diffusion kinetics in garnet: experimental studies and appications. Geochimica et Cosmochimica Acta 69, 2385–2398.

Tomkins, H.S., Powell, R., Ellis, D.J., 2007. The pressure dependence of the zirconium-in-rutile thermometer. Journal of Metamorphic Geology 25, 703–713.

Van Orman, J.A., Grove, T.L., Shimizu, N., Layne, G.D., 2002. Rare earth element diffusion in a natural pyrope single crystal at 2.8 GPa. Contributions to Mineralogy and Petrology 142, 416–424.

Weller, O.M., St-Onge, M.R., 2017. Record of modern-style plate tectonics in the Paleoproterozoic Trans–Hudson orogeny. Nature Geoscience 10, 305–311.

White, R.W., Powell, R., 2002. Melt loss and the preservation of granulite facies mineral assemblages. Journal of Metamorphic Geology 20, 621–632.

White, R.W., Powell, R., Holland, T.J.B., 2001. Calculation of partial melting equilibria in the system Na2O–CaO–K2O–FeO–MgO–Al2O3–SiO2–H2O (NCKFMASH). Journal of Metamorphic Geology 19, 139–153.

Whitney, D.L., Evans, B.W., 2010. Abbreviations for names of rock-forming minerals. American Mineralogist 95, 185–187.

Wiedenbeck, M., Allé, P., Corfu, F., Griffin, W.L., et al., 2010. Three natural zircon standards for U-Th-Pb, Lu-Hf, trace element and REE analyses. Geostandards Newsletter 19, 1–23.

Wu, F.Y., Yang, Y.H., Xie, L.W., Yang, J.H., Xu, P., 2006. Hf isotopic compositions of the standard zircons and baddeleyites used in U-Pb geochronology. Chemical Geology 234, 105–126.

Xu, C., Kynický, J., Tao, R., Liu, X., Zhang, L., Pohanka, M., et al., 2017. Recovery of an oxidized majorite inclusion from Earth's deep asthenosphere. Science Advances 3, e1601589.

Yang, Y.H., Zhang, H.F., Chu, Z.Y., Xie, L.W., Wu, F.Y., 2010. Combined chemical separation of Lu, Hf, Rb, Sr, Sm and Nd from a single rock digest and precise and accurate isotope determinations of Lu-Hf, Rb-Sr and Sm-Nd isotope systems using Multi-Collector ICP-MS and TIMS. International Journal of Mass Spectrometry 290, 120–126.

Yu, H.L., Zhang, L.F., Wei, C.J., Li, X.L., Guo, J.H., 2017. Age and P-T conditions of the Gridino-type eclogite in the Belomorian Province, Russia. Journal of Metamorphic Geology 35, 855–869.

Yu, H.L., Zhang, L.F., Wei, C.J., Li, X.L., et al. The metamorphic evolution of Salma-type eclogite in Russia: constraints from zircon/titanite dating and phase equilibria modeling. Precambrian Research, (under review).

Zhao, G.C., Cawood, P.A., Wilde, S.A., Sun, M., 2002. Review of global 2.1–1.8 Ga orogens: implications for a pre-Rodinia supercontinent. Earth-Science Reviews 59, 125–162.